J. Hydrol. Hydromech., 73, 2025, 4, 412–442
https://doi.org/10.2478/johh-2025-0032

Journal of Hydrology and Hydromechanics

Equilibrium scour pattern around tandem piers at an intermediate below-critical inflow velocity

Harshvardhan, Deo Raj Kaushal*

Department of Civil Engineering, Indian Institute of Technology Delhi, Hauz Khas, New Delhi, India.
* Corresponding author. E-mail: kaushal@civil.iitd.ac.in

Abstract: Scouring around bridge piers is one of the major reasons for bridge failure. A total of 20 experiments of scour around tandem piers were conducted in an open channel, at a subcritical inflow velocity (U/U_c=0.67) by placing an equal or smaller diameter circular bridge pier downstream of an existing pier with relative diameters in the range 1.00 to 0.67, at varied normalized spacings in the range 4 to 9.33, and detailed measurements of the equilibrium scour beds were taken. Separate scour holes with distinct deposition between the piers was observed in the majority of cases. Highest reinforcement effects were observed for pier combinations with Dd/Du=0.90 and 0.80, resulting in larger scour hole dimensions at the upstream pier, compared to isolated condition. The spacing corresponding to the minimum scour hole dimensions at the downstream pier was observed in the range L/Du=4 to 9.33 for each pier combination and it decreased with the decrease in diameter of the downstream pier. Variations for the normalized equilibrium scour depth, lateral and longitudinal extents of the scour hole, scour surface area, and scour hole volume as a function of normalized spacing for different ratios of downstream and upstream pier diameters, are presented in the form of graphs and equations.

Keywords: Inline bridge piers; Scour; Volume; Area; Longitudinal Extent; Lateral Extent; Unidentical Piers; Equilibrium scour; Low inflow velocity.

1 INTRODUCTION

Piers supporting the bridges are susceptible to failure due to local scour. It is thus essential to be able to predict the scour hole dimensions to determine the extra depth of foundation required for stability. The essential elements of flow field around a pier comprises of downflow at the upstream pier face, horseshoe vortices that wrap around the base of the pier and wake vortices at the downstream of the pier. These vortex structures create hydrodynamic forces on the sediment particles, which are entrained into the flow and move in different trajectories before settling again. This leads to local deposition and erosion patterns. As a result, a scour hole is developed due to the removal of bed sediments. The scour mechanism around tandem piers is more complex than isolated piers due to the mutual interaction of the flow structures, and comprises of four distinct mechanisms proposed by Hannah (1978), viz., reinforcing, sheltering, shed vortices and compressed horseshoe vortex. The downstream pier affects the scour hole dimensions around the upstream pier by reinforcement, i.e., by lowering the bed level between the piers, thus easing the sediment removal around the front pier as shown in Figure 1(b). The upstream pier influences the scour at a downstream pier by modifying the flow field in the wake flow region which acts as an incoming flow for the downstream pier and feeds the scour hole of the downstream pier through its eroded sediments (Khaple et al., 2017). This leads to the sheltering of the downstream pier. A possible flow field scenario and scour holes around the two piers is shown in Figure 1(a).

Till now, nearly all studies on scour around tandem piers have been carried out at inflow velocities close to the critical velocity of incipient motion of sediment particles with U/U_c in the range 0.9 to 1. However, flow in the water body is unpredictable and variable. Thus, velocities below the critical value are expected in the field. While the effect of velocity on the equilibrium scour hole dimensions around isolated piers is largely established by various studies such as Arneson et al. (2012), Chiew (1995), Dongguang et al. (1993), Harshvardhan and Kaushal (2025), Melville and Chiew (1999), Sheppard et al. (2004), etc., the effect of velocity on scour around tandem bridge piers is largely unknown. The present study, by carrying out scour studies on identical and unidentical tandem piers, at a significantly lower velocity below the critical velocity, with U/U_c = 0.67, attempts to explore the effect. Additionally, for the chosen flow velocity, the pier to pier spacing and the diameter of the downstream pier is varied to establish the effect of spacing and relative diameters on the equilibrium scour hole pattern around the two piers.

Due to the rapid pace of urbanization and increase in traffic volume, it is often necessary to erect new bridges in close proximity to an existing bridge since land acquisition is difficult (Beg, 2008, Khaple et al., 2017; Rahul, 2021). Scour studies on two inline identical piers have been carried out by Ashtiani and Beheshti (2006), Beg (2004), Devi and Kumar (2022), Dietz (1973), Hannah (1978), Kehsavarzi et al. (2018), Khaple et al. (2017), Nazariha (1996), Malik and Setia (2021), etc., in the past. These studies are restricted to identical piers. If the new bridge is to be designed to withstand lighter loads with shorter spans than the existing bridge, smaller piers are sufficient to ensure safety and stability. During placement of piers, it is a likely possibility that a smaller sized bridge pier of the newly constructed bridge falls in line with a larger sized pier of an existing bridge along the flow direction as the smaller diameter piers are closely spaced while larger sized piers are spaced farther apart (Beg and Beg, 2015). The current study attempts to determine scour hole geometry around inline unidentical circular piers with the lower diameter pier placed on the downstream side of a fixed higher diameter pier. The construction of new bridge piers downstream of an existing bridge also affects the scour hole dimensions around the upstream bridge piers. Therefore, appropriate and sufficient countermeasures should be provided for the existing upstream bridge piers to prevent their failure due to the construction of the new bridge piers. Moreover, majority of the mentioned studies focuses on a single value of the equilibrium scour depth at the front of the piers. However, the scour hole's volume, surface area, slope, and longitudinal and lateral extents are all equally significant features that indicate its severity and specify the necessary countermeasures (Yanmaz and Kose, 2007). By examining the geometric properties of the scour hole created and putting out equations for the same, the current work gets over this drawback of earlier research.

The main objective of the present study is to carry out experiments on identical and unidentical inline circular pier models, changing the spacing between them and obtaining non-dimensional scour hole dimensions in the form of graphs and equations. A limited number of cases (24) are taken up in this study keeping field conditions in mind and also to help the capture of detailed measurements of the equilibrium scour bed to help the bridge designer make a more informed decision.

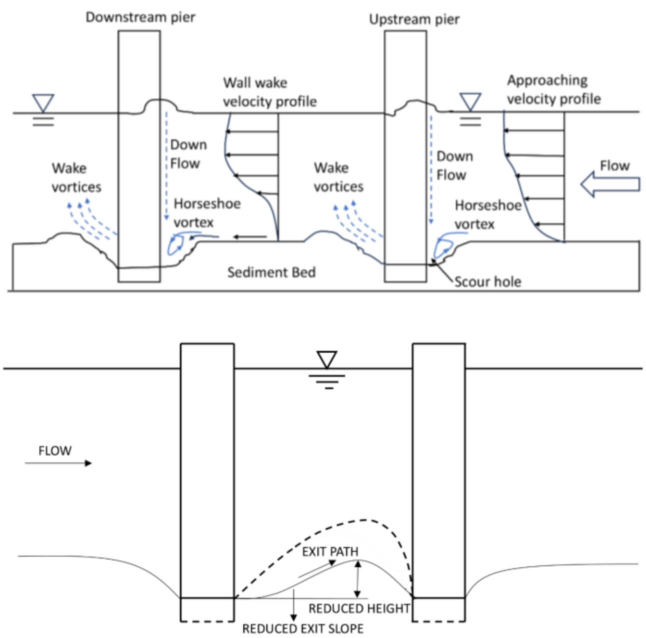

Fig. 1. (a) Schematic diagram of scour holes and flow field around two piers in tandem arrangement (Khaple et al. 2017) (upper figure); Reinforcement effect (Nazariha, 1996) (lower figure).

2 EXPERIMENTAL SETUP

A laboratory channel of dimensions 7.89 m x 0.15 m x 0.19 m (Length x Breadth x Height) with sidewalls made of plexiglass was used in the study. The tailwater depth was maintained using a sharp-crested overflow weir fitted at the downstream end of the channel. The discharge in the channel was regulated using a valve and an electromagnetic flow meter fitted in the channel. The test section was 1.4 m long and 5 cm deep and was positioned 5.55 m downstream from the inlet of the channel. Solid circular stainless-steel cylinders of diameters 10 mm, 12 mm, 13.5 mm and 15 mm were used as pier models. The channel width should be at least 10 times the pier width to avoid the contraction effect as suggested by Melville and Coleman (2000). Therefore, the maximum diameter of pier was taken as 15 mm. Also, the low inflow velocity with U/U_c = 0.67 ensured that the scour hole dimensions were well inside the width of the flume resulting in negligible secondary flow effects. The details of the experimental setup have also been described in Harshvardhan and Kaushal (2025), which was carried out for isolated piers. The 4 runs for isolated piers at U/U_c = 0.67 carried out in Harshvardhan and Kaushal (2025) have been used as reference to establish the effect of placing a downstream pier at varied distances. The schematic of the setup for inline piers is shown in Fig. 2 for two inline piers. In all experiments of this series the upstream pier was located at 5.85 meter from the inlet of the flume and only the downstream pier was moved to set it at the desired pier spacing in the next experiment. Fig. 2 (a) shows the plan of the channel with different segments filled with different materials from inlet to the outlet. The thickness of each segment was kept as 5 cm. The working section was 1.40 m long at the middle part of the channel. At first, stainless steel cylinders fitted into rectangular base plates (130 mm x 50 mm x 9 mm), were placed in the working sections at the desired spacing. Then sand was filled and compacted in layers of 1 cm up to a total thickness of 5 cm. At the inlet, a honeycomb flow straightener was fitted to minimize turbulence in the flow. The first 5.55 m of the channel was filled with 10–20 mm sized gravel in order to generate fully developed flows. The turbulent boundary layer thickness along a smooth flat plate is given as (Schlichting, 1979): $\delta(x) = 0.37x\frac{Ux}{\nu}^{-0.2}$ in which $x =$ longitudinal distance, U = free stream velocity, and ν = kinematic viscosity (=10^{-6} m²/s). The free velocity at section x = 5.55 m into the channel was measured at 0.189 m/s. Substituting these values of x and U, the boundary layer thickness at this point in the test section becomes $\delta(x) = 0.128$ m, which is greater than the mean flow depth = 0.11 m. Thus, the turbulent boundary layer extends across the entire flow depth, and flow is fully developed in the test section. The size of the sediments, starting from inlet, was gradually reduced from gravel to fine gravel (5 mm-10 mm) to sand and then gradually increased to fine gravel to gravel, till the outlet as shown in Figure 2(a) and 2(b). To obtain highly uniform sand, available sand was sieved between 425-micron and 500-micron sieves, and the sand passing through the 500-micron sieve and retained on the 425-micron sieve was used to prepare the bed. The median size of the sand particles, d_{50}, is therefore taken as the mean of the two sieve sizes i.e., 462.5 microns. The specific gravity of the sediment was 2.65 t/m^3, with an angle of repose $\varphi = 33.34°$. The slope of the test bed was set to $S_0 = 0.0002$. The effect of water depth and sediment size was attempted to be nullified by adopting water depth and sediment size such that $h/D > 4$ and $D/d_{50} > 20$ as suggested by Ettema (1980) and also adopted by Nazariha (1996) in his study for similar sizes of pier and sediment as the present study. In the present study, minimum value of h/D corresponds to D=15 mm and is equal 110/15 = 7.33 and the minimum value of sediment coarseness, D/d_{50} corresponds to $D = 10$ mm and is equal to 10/0.462=21.64>20. However, if the size of sediment and depth of flow exceed the accepted limiting values, their effects on local scour depth are documented. The appropriate correction factors must be applied accordingly (Nazariha, 1996).

The flow parameters are provided in Table 1. In all cases of piers in tandem arrangement, the largest diameter pier i.e., 15 mm was placed on the upstream side. At the downstream side, piers of diameters 10 mm, 12 mm, 13.5 mm and 15 mm were placed. Thus, the ratios of D_d/D_u were taken as 1.00, 0.90, 0.80 and 0.67. The piers were placed such that the angle of attack of flow was zero in each case. The piers were positioned at the centerline of the channel. For the tandem arrangement of piers, the spacing between the piers was varied in increments of 20 mm with absolute values 60 mm, 80 mm, 100 mm, 120 mm and 140 mm resulting in L/D_u values of 4, 5.33, 6.67, 8 and 9.33. Experiments were carried out upto the spacings for each pier combination at which the first noticeable increase in scour depth at the downstream pier was observed so as to locate the point of minima of scour depths at the downstream pier. The reason behind limiting the spacings to $L/D_u = 9.33$ is because as we will see in the subsequent section that we reach a point where scour depth at the downstream pier starts increasing. Therefore, it is economically more feasible to place the second downstream bridge pier within this range to have the maximum advantage of the upstream pier shielding the downstream pier, thereby removing the additional cost burden associated with designing the foundation of the downstream bridge pier for the extra depth. The ratio of downstream and upstream piers was taken in the range 0.67 to 1.0 to cover probable capacity of new bridge required, especially when both bridges are operational. The normalized spacing between the piers was taken in the range 4 to $9\frac{1}{3}$ because the second bridge will be a little far away from the first bridge and low normalized spacings in the range 0–4 are expected to be achieved for identical piers of the same bridge for which many studies have been conducted in the past, although at near critical flow velocities.

A total set of 20 experiments using two piers in tandem arrangement (20 experiments) with various spacings were performed for a duration of 600 mins. The span of the experiments was 600 mins as very little to no sediment motion in the vicinity of the piers was noticed after this duration. Each configuration was tested under the same flow conditions as shown in Table 1. The critical velocity, U_c, at which sediment initiates motion was calculated using the equation proposed by Melville and Coleman (2000). Each experiment was monitored for the time variation of scour depth and readings were noted at different intervals of time. The temporal developments at front of 15 mm upstream pier and 13.5 mm downstream pier at a spacing of 60 mm are shown in Fig. 2 (e). It can be seen from the figure that scour is developed rapidly during the initial phase at the front of the piers and the rate of scour decreases with time. The scour depths were taken on a grid of 4mm x 4mm (x x y) for the scoured region and 10mm x 4mm (x x y) for the deposition region, using a vernier point gauge with a least count of 0.1 mm.

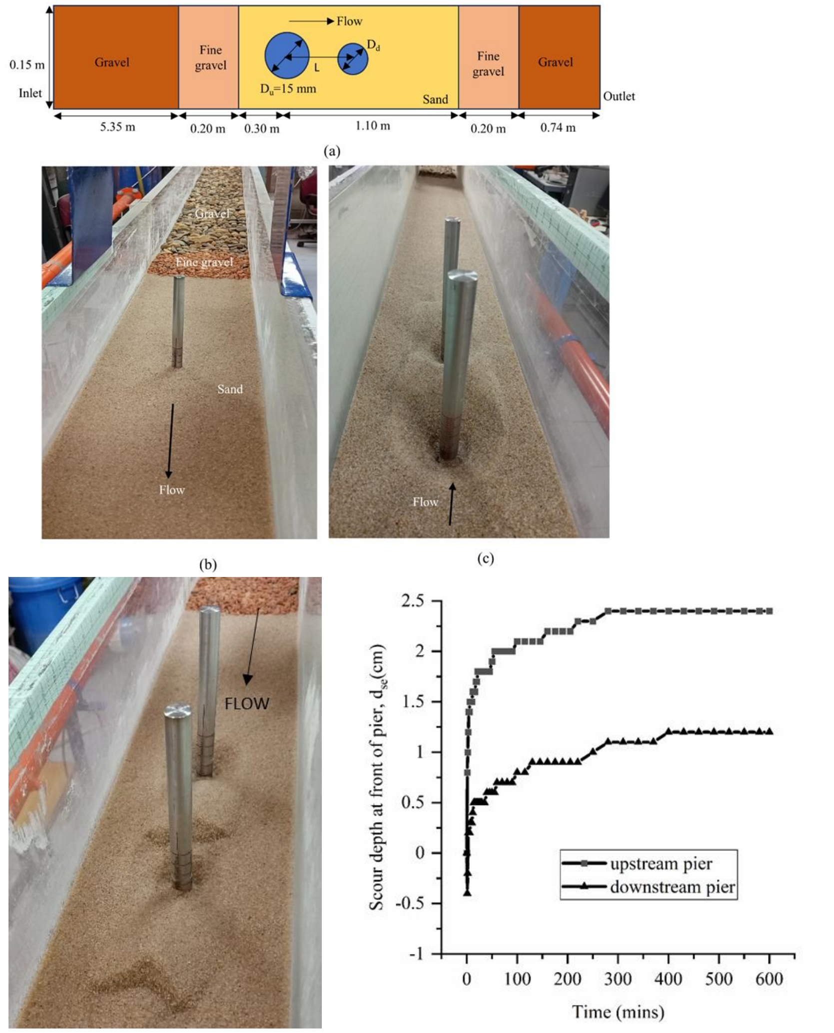

(d) (e)

Fig. 2. (a) Plan of the channel (b) photograph depicting different segments of the bed (c) photograph showing the equilibrium scour depth for tandem piers with $D_d/D_u = 0.80$ at $L/D_u = 6.67$ (d) photograph showing the equilibrium scour depth for tandem piers with $D_d/D_u = 1.00$ at $L/D_u = 9.33$ (e) Time evolution of the scour depth at the front of 15 mm upstream pier and 13.5 mm downstream pier with a spacing of 60 mm

Table 1. Flow parameters.

Q (m^3/s)	H (m)	d_{50} (mm)	U_c (m/s)	U (m/s)	U/U_c
0.00311	0.11	0.462	0.282	0.189	0.67

3 RESULTS AND DISCUSSION

3.1 Scour Hole Measurements

3.1.1 Maximum scour depths

The major distinction of the present study with other similar studies is that the present study is carried out at $U/U_c = 0.67$, while the other similar studies are conducted at U/U_c in the range 0.9 to 1.0. Therefore, the existing studies cannot be directly compared with the present study, which is carried out at a significantly lower U/U_c. However, comparison of the present study with the existing studies by considering the entire range of spacings reveal the true story.

The variation of scour depths at the upstream and downstream piers for U/U_c in the range 0.9-1.0 conducted by most studies are described here. For the normalized equilibrium scour depth at the upstream pier, most studies report a single maximum at $L/D = 2.5 - 4$ as shown in Figure 3. This is due to the reinforcement effect by the downstream pier, which lowers the bed level between the piers and thus eases sediment removal from the scour hole of the upstream pier. As the spacing increases, the reinforcement effect decreases and is negligible for $L/D \geq 10$ at which the scour depth at the upstream pier approaches that of isolated pier. For the scour at the downstream pier in case of identical tandem piers, the study by Nazariha (1996) covers the maximum range from $L/D = 1\ to\ 40$. For the normalized equilibrium scour depth at the downstream pier, Nazariha (1996) obtained two points of minima at $L/D = 2.5 - 4$ and $L/D = 13$ and one point of maximum at $L/D = 6$ as shown in Figure 4. Nazariha (1996) used the four mechanisms proposed by Hannah (1978) for pier groups, viz., reinforcing, sheltering, shed vortices and compressed horseshoe vortex. As the upstream pier blocks/shelters the impact of direct flow on the downstream pier, the scour depths at the downstream pier are always less than the isolated piers. This sheltering effect is prevalent for the entire spacing range. At $L/D = 1$, when the piers are touching each other, they behave as an isolated pier and both upstream and downstream piers have scour depth equal to that of isolated pier, resulting in normalized scour depth equal to 1. From $L/D = 1$ to the point of first minima, Nazariha (1996) found that the scour depth at the downstream pier decreased since the downstream pier still lies inside the scour hole of the upstream pier. For $L/D \geq 5$, Nazariha (1996) found that the upstream and downstream piers had independent scour holes. After the point of first minima scour depth at the downstream pier started to increase as the, the interaction between wake vortices of the upstream pier and vortex systems of the downstream pier kept the particles in suspension and did not let the particles to deposit inside the scour hole of the rear pier. Thus, scour depth increased till the maximum at $L/D = 6$. After the point of maximum, the vortex interaction started to weaken and sheltering effect was still dominant, causing the scour depth to continue to decrease till the point of second minimum after which the sheltering effect started to weaken and sediment transport into the downstream hole ceased, the deposition mound of the upstream pier ended before the position of the downstream pier and scour depths again started to increase. In the present study, sediment transport into the downstream scour hole from the upstream had ceased and the deposition mound of the upstream pier ended before the downstream pier after $L/D >$ 6.67 and scour depth at the downstream pier started to increase. thus, we had reached the point of second minimum as shown in Figure 2(d) for identical tandem piers at $L/D = 9.33$.

As seen in Figure 4, the L/D corresponding to the second minimum for d_{sed}/d_{sei} vs L/D curve is found to be in the range 13-14 by Nazariha (1996), Beg (2004) and Malik and Setia (2021), 8 by Khaple et al. (2017) and 6.67 in the present study. The change in the location of minimum is primarily due to the difference in the ratio of inflow and critical velocities used in the different studies. As shown in table 2, Studies by Beg (2004), Malik and Setia (2021) and Nazariha (1996) were conducted at $U/U_c = 0.9 - 1.0$ and had the highest L/D corresponding to the second minimum equal to 13–14. While Khaple et al. (2017) claimed to have conducted studies at $U/U_c = 0.9$, upon applying the widely accepted formulation for computing critical velocity by Melville and Coleman (2000), it was found that the value of U/U_c was 0.82 for $d_{50} = 1.8$ mm and $h = 160$ mm. Khaple et al. (2017) observed the location of minimum to be at $L/D = 8$. The present study which is carried out at $U/U_c = 0.67$, found the location of minimum to be at $L/D = 6.67$. Thus, clearly as the inflow velocity increases, the location of second minimum moves farther downstream. This is because, the higher flow causes greater scour at the upstream pier whose particles are able to travel farther downstream and deposit inside the hole of the downstream pier up to a farther spacing, causing a reduction in scour depth at the downstream pier up to a larger spacing between the piers. Thus, minimum is observed at a farther spacing. Since, most studies are conducted at near critical velocities ($U/U_c = 0.9 - 1.0$), this phenomenon has not been observed in earlier studies. Also, it is seen that the magnitudes of normalized scour depths, i.e., d_{sed}/d_{sei} are different across studies. The present study agrees closely with the curve of Nazariha (1996) with the minimum of the curve shifted from $L/D = 13$ to $L/D = 6.67$ due to the change in value of U/U_c from 0.9-1.0 to 0.67. Studies by Hannah (1978) and Beg (2004) agree well with each other, while the study by Malik and Setia (2021) report the highest values of normalized scour depths enveloping all other studies. This is because the present study and that by Nazariha (1996) are conducted for similar pier sizes i.e., 10 mm and 12.7 mm and at similar D/d_{50}, i.e., 21.62 and 26.5 respectively. The data of Beg (2004) is consistent with that of Hannah (1978) since they are carried out at similar D/d_{50}, i.e., 35 and 44 respectively and also identical pier size, i.e., 33 mm. The study by Malik and Setia (2021), was carried out at an extremely large ratio of D/d_{50}, i.e., 270, and thus envelops all curves with the highest normalized scour depths reported for the entire range of spacings. These studies suggest that scour depth at the downstream pier increases with increasing D/d_{50}.

Table 2. Comparison of inflow velocities and location of second minimum in different studies.

S. No.	Studies	U/U_c	L/D of min d_{sed}/d_{sei}
1	Nazariha (1996), Beg (2004), Malik and Setia (2021)	0.9-1.0	13-14
2	Khaple et al. (2017)	0.82 (as per Melville and Coleman (2000) formula)	8
3	Present Study	0.67	6.67

For the upstream pier, around the point of second minimum, there was little to no effect on the upstream pier resulting in values of normalized scour depths close to unity. Since the present study and the study by Khaple et al. (2017) are carried out at lower values of U/U_c, and around the second minimum, both report minimal effect of the downstream pier on the scour depth at the upstream pier, as shown in Figure 3.

The results for the 24 tests are presented in Table 2, in which d_{sei} and d_{seu} are the equilibrium scour depths at the front of an isolated pier and the upstream pier in case of two tandem piers, respectively, while d_{sed} is the equilibrium scour depth at the front of the downstream pier for tandem piers. The ratios d_{seu}/d_{sei} and d_{sed}/d_{sei} are correction factors to be applied to the isolated pier scour depths at the upstream and downstream pier to obtain the corresponding values when they are placed in tandem with another pier. It is to be noted that all the spacings have been normalized with respect to the diameter of the upstream pier, as the diameter of the upstream pier is same for all pier combinations, i.e., 15 mm.

As seen through Figure 5 (a), for all pier combinations ($D_d/D_u = 1.00$, 0.90, 0.80 and 0.67), there is reinforcement effect seen on the upstream pier due to the presence of the downstream pier, which increases the scour around the upstream pier reflected in greater than unity normalized scour depths shown in Figure 5 (a) and Table 3. This effect seems to decrease with the increase in spacing for all cases, as is observed by nearly all other studies for identical tandem piers. In terms of observed normalized equilibrium scour depths at the upstream pier, it is seen that the normalized scour depths at the upstream pier when a smaller sized pier is placed downstream, i.e., $D_d/D_u < 1$, is generally higher than the corresponding values when an identical-sized pier is placed downstream, i.e., $D_d/D_u = 1$. Amongst the unidentical pier combinations, cases with $D_d/D_u = 0.90$, i.e. when the downstream pier is slightly lower in size than the upstream pier, report the highest normalized scour depths at the upstream pier followed by $D_d/D_u = 0.80$, followed by $D_d/D_u = 0.67$. Thus, the reinforcement effect at the upstream pier seems to decrease with the decrease in diameter of the downstream pier in terms of normalized scour depth values. This is because as the size of downstream pier gets reduced, so does the scour depth between the piers, therefore, the particles eroded from the upstream pier find it difficult to cross the relatively steeper downstream slope of the upstream scour hole and therefore scour at upstream pier is reduced.

As seen in Fig. 5(b), for the downstream pier, for any pier combination ($D_d/D_u = 1.00$, 0.90, 0.80 and 0.67), the normalized equilibrium scour depth either remains constant or decreases with increase in spacing up to a threshold spacing after which the scour depth starts increasing. The L/D_u corresponding to the minimum normalized equilibrium scour depths at the downstream pier is found to be 6.67 for $D_d/D_u = 1.00$, 8 for $D_d/D_u = 0.90$, (6.67-8) for $D_d/D_u = 0.80$ and (4-8) for $D_d/D_u = 0.67$. Thus, for unidentical piers, the point of minima seems to move upstream closer to the upstream pier with decrease in diameter of the downstream pier. Moreover, sharper minima points are observed for higher $D_d/D_u = 1.00$ and 0.90, while flatter (spread over a larger L/D_u range) minima are observed for pier combinations with lower sized downstream piers, i.e., $D_d/D_u = 0.80$ and 0.67. In fact, the normalized scour depths remain nearly constant from $L/D_u = 4\ to\ 8$ for pier combination with the smallest downstream pier with $D_d/D_u = 0.67$. This may be due to the inability of the smaller sized piers in causing sharp changes in scour depths at the downstream pier with the change in spacing. Clearly, the slope of fall for $D_d/D_u = 0.90$ is sharper and gets flatter with decrease in diameter of the downstream pier to $D_d/D_u = 0.80$ and then very flat to $D_d/D_u = 0.67$. However, after the end of minima range for all pier combinations with a smaller sized downstream pier ($D_d/D_u < 1$) at $L/D_u = 8$, the normalized equilibrium scour depth at the rear pier for the pier combination with the lowest downstream pier size ($D_d/D_u = 0.67$), report the sharpest increase followed by $D_d/D_u = 0.80$, followed by $D_d/D_u = 0.90$, as evident from the slopes of the curves from $L/D_u = 8$ to $L/D_u = 9.33$ in Fig. 5(b). This reflects that the ability of a smaller sized downstream pier to regain its scour depth, for the same increase in spacing after the sheltering effect of the upstream pier subsides and its deposition region ends before the start of the downstream pier, increases with the decrease in the diameter of the downstream pier. Due to the above reasons, it is seen in Fig. 5(b) that the curves for different pier combinations at downstream pier are not entirely above or below each other for the entire range of spacings and cross each other at some point. For convenience of application, polynomials are fit for the variation of normalized scour depths at the upstream and downstream piers with normalized spacings and presented in supplementary Tables S1–S4, along with R^2 values.

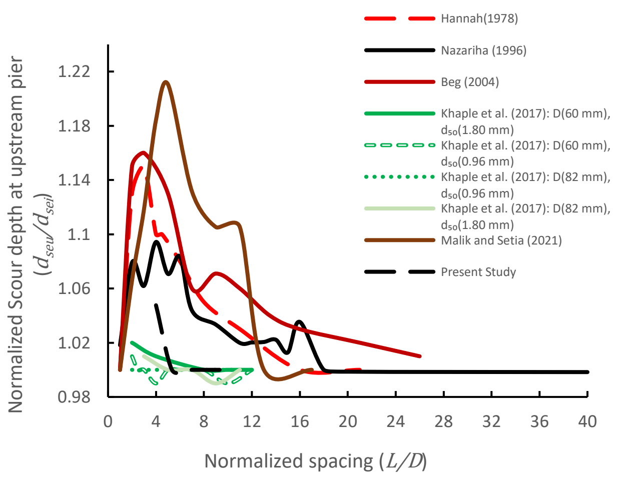

Fig. 3. Comparison of observed normalized scour depths at the upstream pier with different studies in literature.

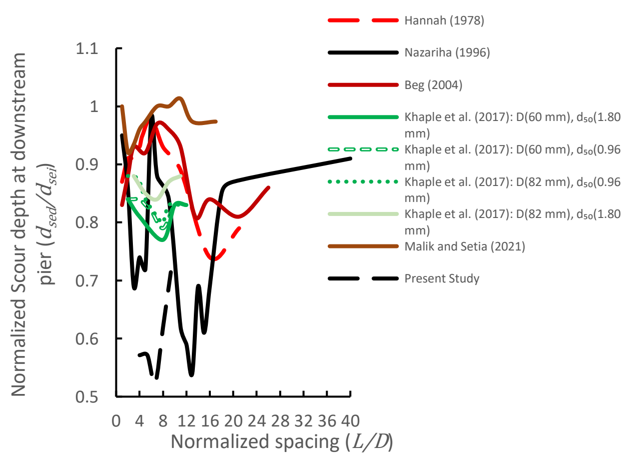

Fig. 4. Comparison of observed normalized scour depths at the downstream pier with different studies in literature.

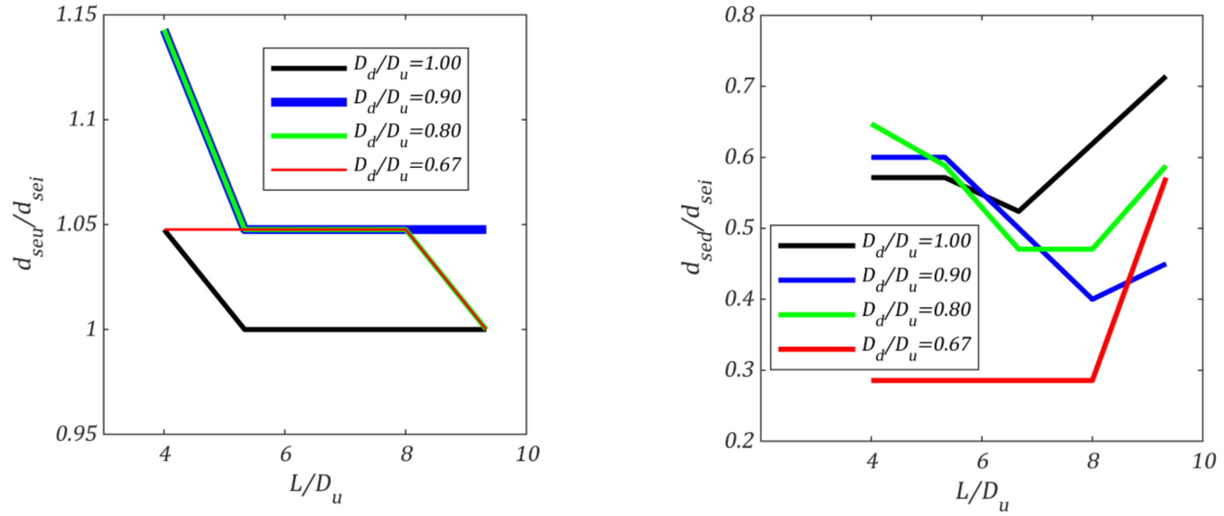

Fig. 5. Variation of the Normalised Equilibrium Scour depth at the front of (a) upstream pier and (b) downstream pier for different normalized spacing values for $D_d/D_u = 0.67\ to\ 1.00$

Table 3. Equilibrium scour depths of different cases.

Run No.	D_u (mm)	D_d (mm)	L/D_u	d_{seu} or d_{sei} (mm)	d_{sed} (mm)	d_{seu}/d_{sei}	d_{sed}/d_{sei}
1	10	NA	NA	14	NA	NA	NA
2	12	NA	NA	17	NA	NA	NA
3	13.5	NA	NA	20	NA	NA	NA
4	15	NA	NA	21	NA	NA	NA
5	15	15	4	22	12	1.048	0.571
6	15	15	5.333	21	12	1.000	0.571
7	15	15	6.667	21	11	1.000	0.524
8	15	15	8	21	13	1.000	0.619
9	15	15	9.333	21	15	1.000	0.714
10	15	10	4	22	4	1.048	0.286
11	15	10	5.333	22	4	1.048	0.286
12	15	10	6.667	22	4	1.048	0.286
13	15	10	8	22	4	1.048	0.286
14	15	10	9.333	21	8	1.000	0.571
15	15	12	4	24	11	1.143	0.647
16	15	12	5.333	22	10	1.048	0.588
17	15	12	6.667	22	8	1.048	0.471
18	15	12	8	22	8	1.048	0.471
19	15	12	9.333	21	10	1.000	0.588
20	15	13.5	4	24	12	1.143	0.600
21	15	13.5	5.333	22	12	1.048	0.600
22	15	13.5	6.667	22	10	1.048	0.500
23	15	13.5	8	22	8	1.048	0.400
24	15	13.5	9.333	22	9	1.048	0.450

3.1.2 Centerline Scour Profiles

This section discusses the variation of the scour profile at the line of symmetry. Figure 6 (a) shows the centerline scour profiles for $D_d/D_u = 0.9$ at $L/D_u = 4$. The centerline profiles for all other cases are shown in supplementary figures S1 to S4. The dimensionless X-coordinate i.e. X/D_u has been taken along the x-axis while the dimensionless Z-coordinate i.e. Z/D_u has been taken along the Y-axis. It can be seen that the scour hole is steepest upstream of the front pier. The region between the piers is a combination of the downstream scour profile of the upstream pier and the upstream scour profile of the downstream pier. After the downstream pier the profile resembles that of a parabola similar to that of an isolated pier. There is a peak in the profile between the piers, where the two profiles meet. The location of the peak is found to shift downstream and upwards with the increase in the normalized spacing between the piers. The longitudinal extent of the hole is taken along the line of symmetry from the point of zero scour upstream of the front pier to the first point of zero scour downstream of the rear pier, excluding the deposition region between the piers where the peak is above the plane bed level. The location of the peak from the upstream pier is denoted by x_p, the height of the peak from the plane bed level is denoted by h_p and is positive when peak is above the plane bed level, as shown in Fig. 6 (a). For most of the spacings, it is found that the peak between the piers is above the plane bed level and thus separate longitudinal extents were calculated for the upstream and downstream piers in all those cases. The combined longitudinal extent of the scour holes was normalized with the sum of diameters of upstream and downstream piers, i.e., $D_{piers} = D_u + D_d$, shown by bold lines in Fig. 6(b). The individual separate longitudinal extents of the upstream and downstream piers were normalized with their respective diameters D_u and D_d to provide comparison with the normalized longitudinal extents for the same piers in isolated conditions, reported by Harshvardhan and Kaushal (2025). The normalized longitudinal extents at the upstream pier are shown by solid lines with markers, while the normalized longitudinal extents at the downstream pier are shown with dashed lines with markers in Fig. 6(b). The normalized longitudinal extent for isolated piers at $U/U_c = 0.67$ reported in Harshvardhan and Kaushal (2025) is shown by a dashed black line in the same figure.

It is seen through Fig. 6 (b) that the normalized longitudinal extents for the upstream piers are close to the isolated pier line or above it, while they are significantly below the isolated pier line for the downstream pier for all pier combinations. The curve for the combined extent of the scour hole falls somewhere in between the upstream and downstream pier curves. This is logical because the upstream pier experiences some reinforcement effect causing increase in longitudinal extents at it compared to the isolated piers, while the downstream piers are sheltered from the upstream pier for the range of spacings considered causing decline in longitudinal extent of the hole at the downstream pier. Due to the influence of the downstream pier, the combined normalized extent of the scour hole also falls below the isolated pier line.

Similar phenomenon as observed with normalized scour depths at downstream pier shown in Fig. 5 (b), is also observed for the normalized longitudinal extents at the downstream pier. Sharper minima point is observed for $D_d/D_u = 0.90$ which becomes flatter with decreasing downstream pier size to $D_d/D_u = 0.80$ and then further to $D_d/D_u = 0.67$. It also indicates that the minima move upstream with decrease in diameter of the downstream pier. Also, after the end of minima region at $L/D_u = 8$, similar to normalized scour depth variation, the longitudinal extent reports the sharpest rise for $D_d/D_u = 0.67$ followed by $D_d/D_u = 0.80$ followed by $D_d/D_u = 0.9$. So, for the downstream pier, the results fall in line with observations of equilibrium scour depths. The minima for $D_d/D_u = 1.0$ is observed at $L/D_u = 6.67$ as observed for normalized scour depths as well.

As seen in Fig. 6 (b), for the upstream pier, pier combinations with $D_d/D_u = 0.9$ and $D_d/D_u = 0.8$ report higher than isolated normalized longitudinal extents due to greater reinforcement effect as also observed for normalized scour depths for the upstream pier in Fig. 5(a). The reinforcement effect decreases with the increase in spacing for these two pier combinations, resulting in the decline of longitudinal extents at the upstream pier with spacing. For cases with $D_d/D_u = 1.00$ and $D_d/D_u = 0.67$, the values are close to the isolated pier line or slightly below it and exhibit oscillating behavior due to little to no reinforcement effect of the downstream pier as also observed for equilibrium scour depths. The curves for the longitudinal extent combined scour hole mostly follow the trends of variation at the downstream pier due to lesser variation at the upstream pier owing to smaller reinforcement effect and greater variation at the downstream pier due to larger sheltering effect.

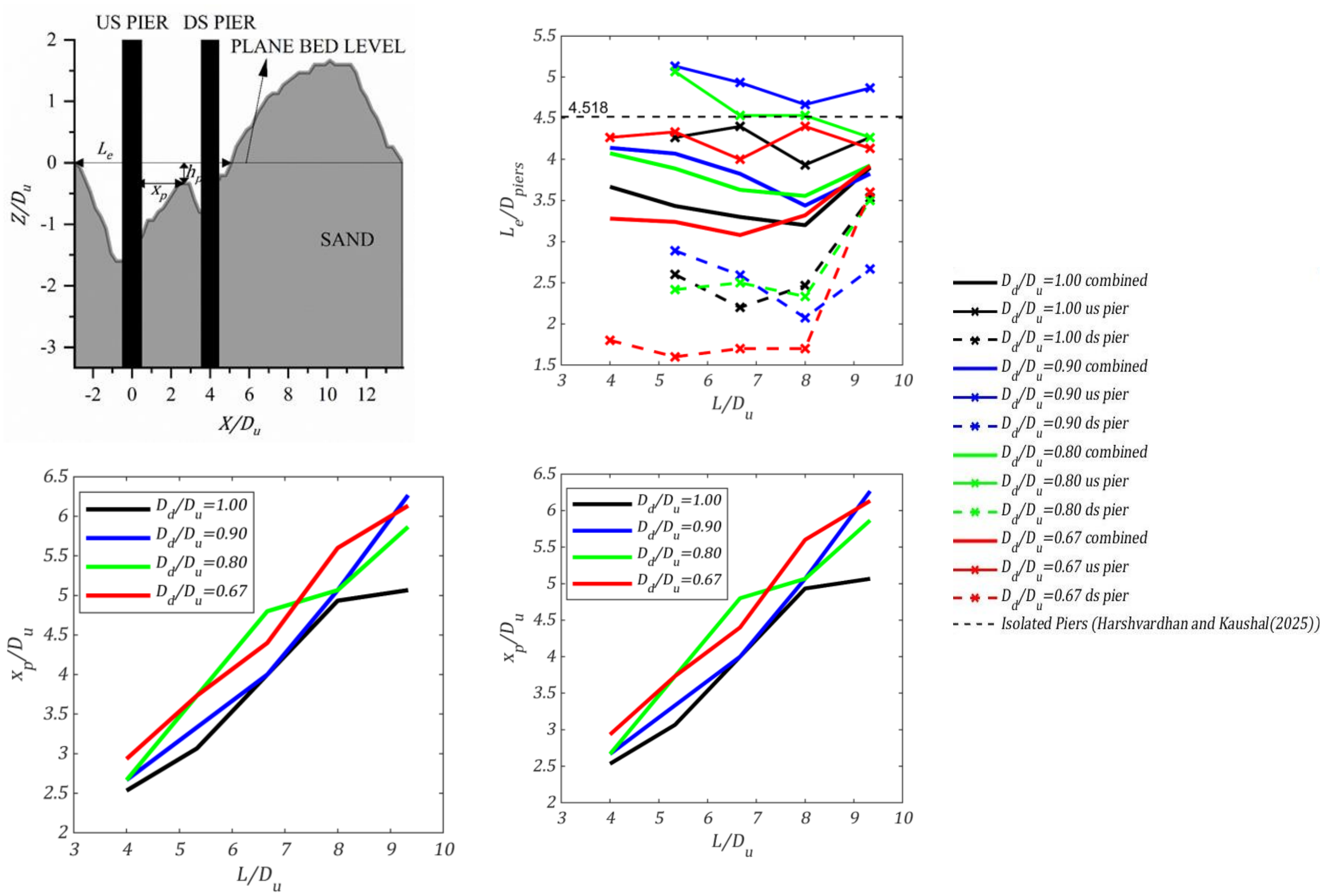

ig. 6. Centerline scour profiles for $D_d/D_u = 0.90$ for $L/D_u = 4$, showing the length of hole L_e, height of peak h_p and location of peak from the upstream pier x_p and best fit curves for Longitudinal extent of combined and individual scour holes at upstream and downstream piers, location and height of peak in the region between the piers vs L/D_u for $D_d/D_u = 1.00\ to\ 0.67$ for L/D_u ranging from 4 to $9\frac{1}{3}$.

As stated before, the height and location of peak between the piers i.e., x_p and h_p both increase with the increase in spacing between the piers for all pier combinations as shown in Figure 6(c) and Figure 6(d). This is because the exit slope of the upstream scour hole gets a greater distance to develop with the increase in spacing between the piers, thus meeting the entry slope of the downstream pier at a farther and higher point. For unidentical pier combinations ($D_d/D_u < 1$), heights of peaks are highest for the pier combination with the smallest sized downstream pier. This is because the exit slope of the upstream scour hole gets a larger distance to reach a greater height when a small sized pier having a small size hole is present at the downstream. Also, for most of the spacings, the location of the peak is also the farthest downstream for $D_d/D_u = 0.67$, and for most part, x_p increases with decreasing D_d/D_u. However, the cases with $D_d/D_u = 0.80$ show higher x_p than $D_d/D_u = 0.67$ for certain spacings, perhaps due to higher reinforcement effect on the upstream pier for these cases as seen through normalized scour depths in Figure 5(a), which pushes the peak downstream. The pier combination with identical piers $D_d/D_u = 1$, report the lowest x_p of all, possibly due to lowest reinforcement effect on the upstream pier as evident from Figure 5(a). However, the heights of peaks for $D_d/D_u = 1$, fall somewhere in between the curves. For convenience of application, polynomials are fit for the variation of longitudinal extent at the upstream, downstream and combined piers, location and height of peak with normalized spacings and presented in supplementary Tables S1-S4, along with R^2 values.

3.1.3 Transverse Scour Profiles

Figures 7(a) and 7(b) shows the transverse scour profiles at the upstream and downstream pier for $D_d/D_u = 0.9$ at $L/D_u = 4$. The dimensionless Y values i.e., Y/D_u are plotted on the x-axis and the dimensionless Z values i.e., Z/D_u are plotted on the y-axis. Transverse profiles at the upstream and downstream piers for all other cases are shown in supplementary figures S5 to S12. From figures, it can be seen that the transverse profile is fairly symmetrical about the pier. The transverse extent of the scour hole has been defined at the pier as the distance between points of zero scour on the left and right sides of the pier with respect to the flow direction. The transverse extents of the scour hole at the upstream and downstream piers, viz., T_u and T_d, were normalized with their respective diameters D_u and D_d to provide comparison with the normalized transverse extents of scour holes for the same piers in isolated conditions, reported by Harshvardhan and Kaushal, (2025). The normalized transverse extents at the upstream and downstream piers are shown in Fig, 7(c) and 7(d), respectively, for different pier combinations. The normalized transverse extent for isolated piers at $U/U_c = 0.67$ reported in Harshvardhan and Kaushal, (2025) is shown by a dashed black line in the two figures.

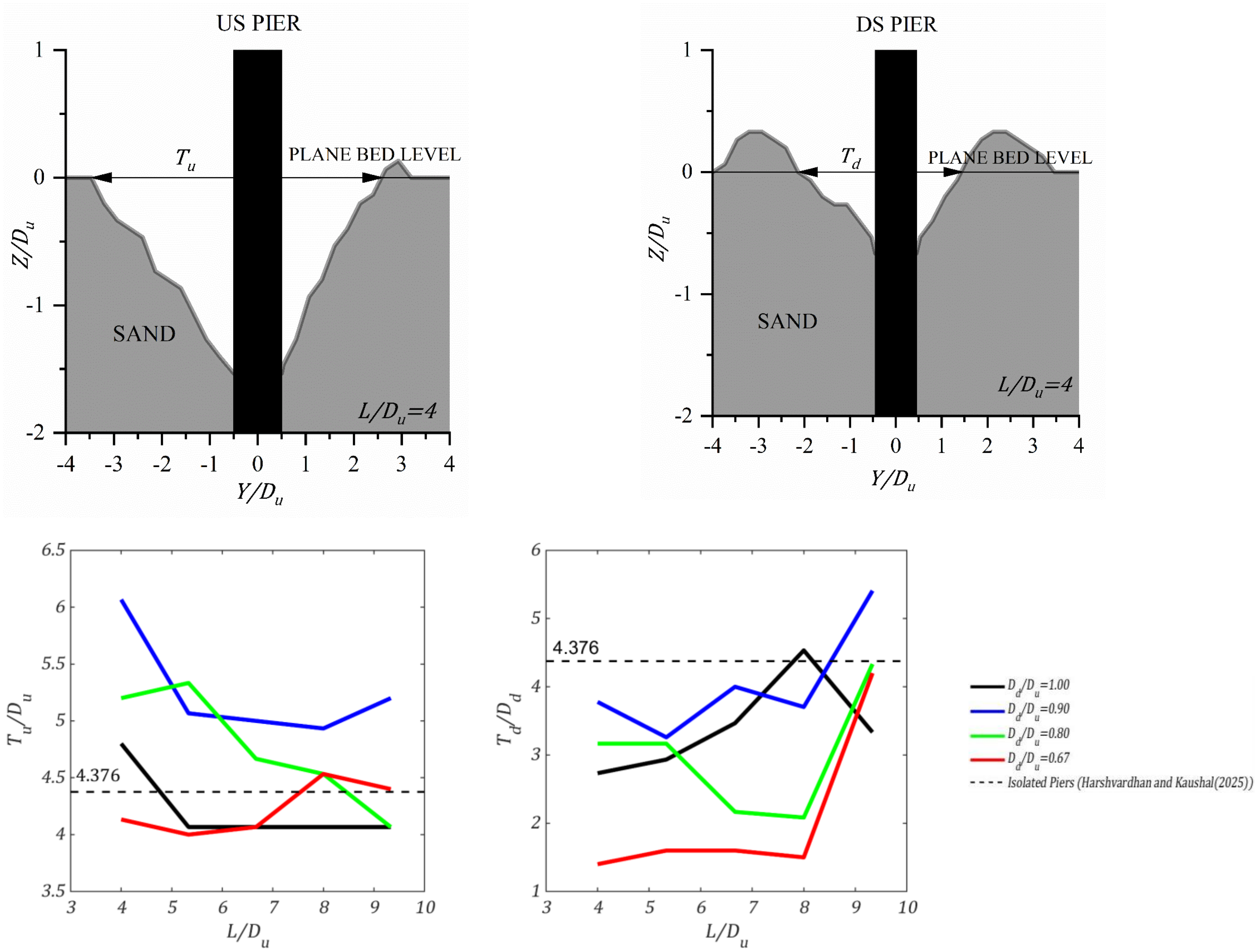

Fig.7. Transverse scour profiles at the upstream and downstream pier for $D_d/D_u = 0.90$ at $L/D_u = 4$, and best fit curves for transverse extents of scour hole at the piers vs L/D_u for $D_d/D_u = 1.00$ for L/D_u ranging from 4 to $9\frac{1}{3}$.

For the upstream pier, as observed for the equilibrium scour depths in Fig. 5(a) and longitudinal extents in Fig. 6(b), the transverse extents at the upstream pier report greater than isolated values for pier combinations with $D_d/D_u = 0.9$ and $D_d/D_u = 0.80$, due to higher reinforcement effects observed for the two cases. On the other hand, near isolated or slightly lower transverse extents are reported for pier combinations with $D_d/D_u = 1.0$ and $D_d/D_u = 0.67$, due to lower reinforcement effects. The variation of transverse extent with spacing for $D_d/D_u = 1.0$ follows almost the exact same pattern as the normalized equilibrium scour depths reported in Fig. 5(a), and the variations for other pier combinations agree for the most part with the normalized depths. While there is general decrease of transverse extent with increase in spacing due to decreasing reinforcement effect for each pier combination, there are occasional increments observed for some cases because the transverse extent of the scour hole at the pier is controlled not only by the equilibrium scour depth at the side of the pier but also the slope of the scour hole at the side of the pier. And it is observed that a deep scour hole is often accompanied by a steep scour hole. So, while a higher scour depth attempts to increase the transverse extent, the accompanied steepness of the scour hole attempts to decrease it. These two opposing factors acting simultaneously causes the variation of the transverse extent of the scour hole to deviate from the variation of scour depths. Additionally, it is seen from comparison with longitudinal extents that the reinforcement effect has greater effect on the transverse extent of the scour hole compared to the longitudinal extent of the scour hole at the upstream pier as the maximum increase from the isolated pier level is around 10 % for the longitudinal extent, while it is around 30 % for the transverse extent.

At the downstream pier, the reported normalized transverse extents are below the isolated pier line due to the sheltering of the downstream pier by the upstream pier. The transverse extents for pier combinations with $D_d/D_u < 1$, were seen to be largely controlled by the diameter of the downstream pier with the smallest $D_d/D_u = 0.67$ pier combination reporting the least transverse extents while the largest $D_d/D_u = 0.9$ pier combination reporting the highest normalized transverse extents at the downstream pier for all spacings. There are steep increments observed at $L/D_u = 8$ as observed for the other previous dimensions of the scour hole, the steepest being observed for $D_d/D_u = 0.67$, followed by $D_d/D_u = 0.80$, followed by $D_d/D_u = 0.90$. The variation with spacing for $D_d/D_u = 0.67$ and $D_d/D_u = 0.80$, fall in line with the variation of normalized depths reported in Figure 5(b). On the other hand, there are increments of transverse extent observed for some range for $D_d/D_u = 0.90$, and nearly opposite trend from equilibrium scour depths is observed for $D_d/D_u = 1$. This is due to the same reason mentioned for the upstream pier that a deep scour hole is accompanied by a steep scour hole, which attempts to decrease the lateral extent despite higher scour depths, and vice versa. This can be seen through the scour profiles at the downstream pier for the two pier combinations with $D_d/D_u = 1$ and $D_d/D_u = 0.9$ in supplementary figs. S6 and S8 respectively. Therefore, a dip in the curve for transverse extent is observed for $D_d/D_u = 1$ despite sharp increase in scour depth reported in Fig. 5(b). For convenience of application, polynomials are fit for the variation of normalized transverse extents at the upstream and downstream piers, and presented in supplementary Tables S1-S4, along with R^2 values.

3.1.4 *Contours, Surface area and Volume of scour hole*

This section discusses the variation of the scour hole contours, scour surface area and volume of the scour holes. Fig. 8 (a) and 8 (b) shows the equilibrium scour hole contours and 3-dimensional coloured equilibrium Scour hole contours (d/D_u), respectively for $D_d/D_u = 1.00$ at $L/D_u = 6.67$. The separate scour holes for the upstream and downstream piers with a clear deposition region between the piers can be clearly seen in the two figures. The equilibrium scour hole contours for all other cases are shown in supplementary figures S13 to S16, while the 3-dimensional colored contours are shown in supplementary figures S17 to S20. The dimensionless X-coordinate i.e., X/D_u has been taken along the x-axis, the dimensionless Y-coordinate i.e. Y/D_u has been taken along the y-axis and the dimensionless Z-coordinate, i.e., Z/D_u has been taken along the Z-axis. Three contours of zero elevation, one inner contour each for the two piers and an outer contour enveloping the two are observed for cases with scour holes separated by a deposition mound. The space between the contours is filled with deposition of sediments. Since we are concerned about the scour hole dimensions only, we have considered the inner zero elevation contour for the purpose of calculating the areas of the individual and combined scour holes. The combined scour surface areas of the scour holes were normalized with the sum of areas of upstream and downstream piers, i.e., $A_{piers} = \pi \frac{D_u^2}{4} + \pi \frac{D_d^2}{4}$, shown by bold lines in Figure 8(c). The individual separate scour surface areas of the upstream and downstream piers were normalized with their respective areas $\pi \frac{D_u^2}{4}$ and $\pi \frac{D_d^2}{4}$ to provide comparison with the normalized scour surface areas for the same piers in isolated conditions, reported by Harshvardhan and Kaushal (2025). The normalized scour surface areas at the upstream pier are shown by solid lines with markers, while the same at the downstream pier are shown with dashed lines with markers in Fig. 8(c). The normalized scour surface area for isolated piers at $U/U_c = 0.67$ reported in Harshvardhan and Kaushal (2025) is shown by a dashed black line in the same Fig. 8(c). The volume of the scour hole is calculated using Delaunay Triangulation in MATLAB, in which a triangular mesh is created over the data points, and then the calculated volumes of the individual triangles are summed up to obtain the total volume. The volume of pier is defined as the volume of pier occupying the flow and is calculated by multiplying the area of the pier in plan with the equilibrium scour depth at the front of the pier. The combined scour volumes of the scour holes were normalized with the sum of volumes of flow occupied by the upstream and downstream piers, i.e., $V_{piers} = \pi \frac{D_u^2}{4} \times d_{seu} + \pi \frac{D_d^2}{4} \times d_{sed}$, shown by bold lines in Fig. 8(d). The individual separate scour volumes of the upstream and downstream piers were normalized with the volumes of flow occupied by the respective piers $\pi \frac{D_u^2}{4} \times d_{seu}$ and $\pi \frac{D_d^2}{4} \times d_{sed}$ to provide comparison with the normalized scour volumes for the same piers in isolated conditions, reported by Harshvardhan and Kaushal (2025). The normalized scour volumes at the upstream pier are shown by solid lines with markers, while the same at the downstream pier are shown with dashed lines with markers in Fig. 8(d). The normalized scour surface area for isolated piers at $U/U_c = 0.67$ reported in Harshvardhan and Kaushal (2025) is shown by a dashed black line in the same Fig. 8(d).

In line with the observations of equilibrium scour depths, lateral and longitudinal extents of the scour holes, the normalized scour surface areas and scour hole volumes for the upstream pier are either above or slightly below the isolated pier line due to varying degrees of reinforcement effect at the upstream pier, while the same for the downstream pier are significantly below the isolated pier line due to sheltering effect at the downstream pier. The curves for the combined surface areas and scour volumes lie somewhere in between the respective curves and are observed to be closer to the curves of the upstream pier's normalized areas and volumes as the contributions of the upstream pier to the combined area and volume the scour hole is significantly higher than the downstream pier. This is true even more for the normalized scour volumes as the combined hole and upstream curves runs parallel very next to each other for $D_d/D_u = 1.00$ and $D_d/D_u = 0.67$.

Upstream pier: As observed for the transverse extent, up to 30 % increase in normalized areas and volumes of the scour hole, compared to isolated piers, are observed due to reinforcement effect at the upstream pier. At the upstream pier, highest reinforcement effects are observed for pier combinations with $D_d/D_u = 0.90$ and $D_d/D_u = 0.80$, which decreases with increasing spacing. The normalized areal and volume curves for pier combinations with $D_d/D_u = 1.00$ and $D_d/D_u = 0.67$ are either very close to the isolated pier line or fall slightly below due to less reinforcement effect at the upstream pier for these two pier combinations. The scour surface area is controlled by the length and transverse extents of the scour hole. The nature of variation of normalized scour surface area with spacing at the upstream pier mostly falls in line with the variation of lengths of scour hole at upstream pier reported in Figure 6 (b). This shows that the length of the scour hole has a greater influence in controlling the nature of variation of scour surface area compared to the width of the scour hole. But, since the transverse extent is enhanced much more than longitudinal extent due to reinforcement effect for pier combinations with $D_d/D_u = 0.90$ and $D_d/D_u = 0.80$, it causes the area curves to shift higher above the isolated pier line for these two pier combinations, as seen in Figure 8 (c). The volume of the scour hole is controlled by the area of scour hole and its depth. It is observed that the variation of areal extent and volume extent at the upstream pier for different pier combinations show very similar nature of variation, as seen through comparison of Figures 8 (c) and 8 (d). Due to decline of scour depths and areas with spacing at the upstream pier for pier combinations with $D_d/D_u = 0.90$ and $D_d/D_u = 0.80$, the nature of variation is similar. For pier combinations with $D_d/D_u = 1.00$ and $D_d/D_u = 0.67$, due to the small variation of scour depths, the normalized volumes follow the same trend as the normalized areas.

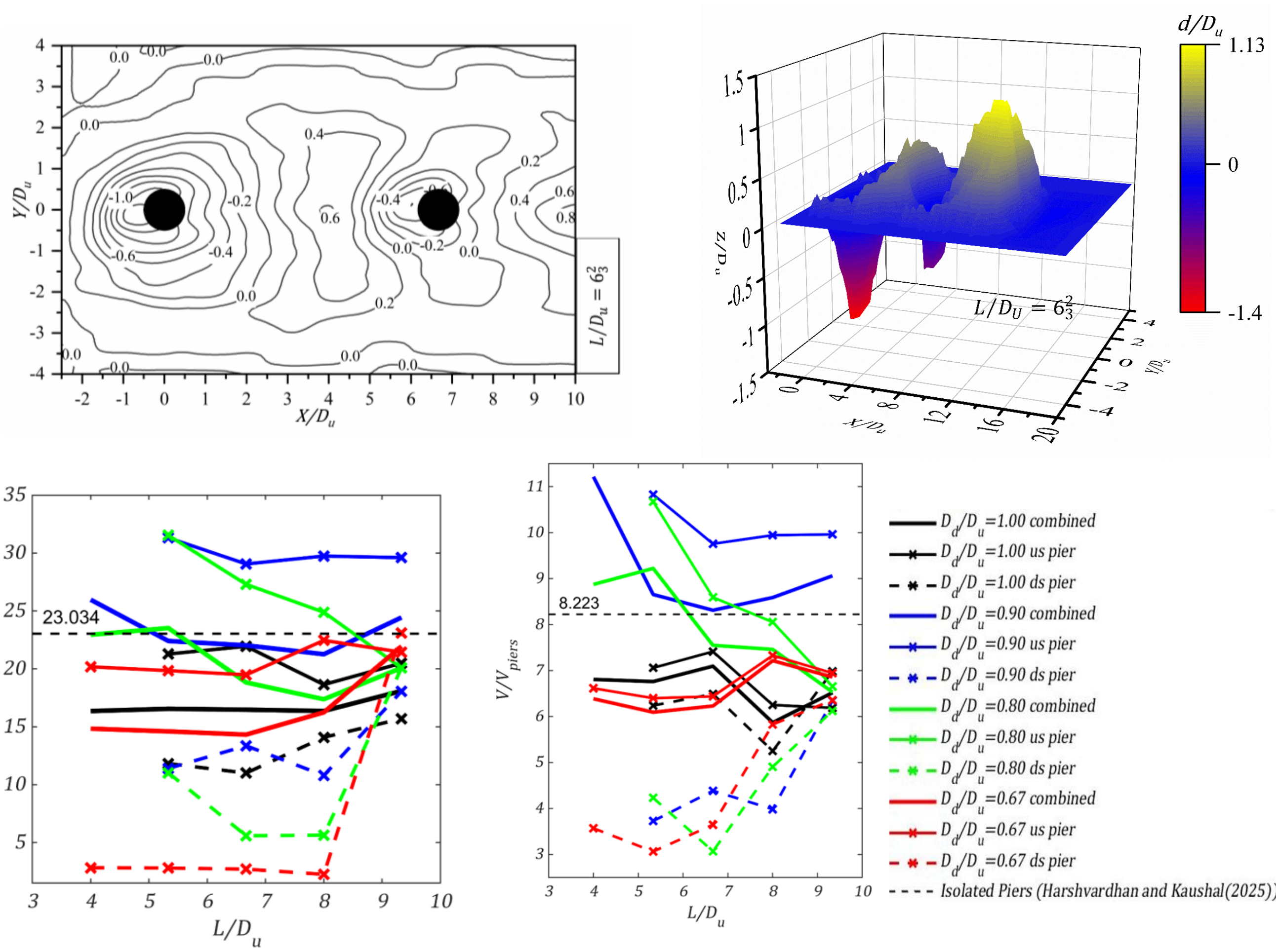

Fig. 8. (a) Equilibrium Scour hole contours (d/D_u) for $D_d/D_u = 1.00$ at $L/D_u = 6.67$ (b) 3-Dimensional Equilibrium Scour hole contours (d/D_u) for $D_d/D_u = 1.00$ at $L/D_u = 6.67$ (c) Variation of normalized combined and individual scour surface area around inline piers at $D_d/D_u = 1.00 \; to \; 0.67$ for L/D_u ranging from 4 to $9\frac{1}{3}$. (d) Variation of normalized combined and individual volume of the scour hole around inline piers for $D_d/D_u = 1.00 \; to \; 0.67$ for L/D_u ranging from 4 to $9\frac{1}{3}$.

Downstream pier: Unlike the upstream pier, the nature of variation of normalized scour surface area with spacing at the downstream pier mostly falls in line with the variation of transverse extents of scour hole at downstream pier reported in Fig. 7 (d) for pier combinations with $D_d/D_u < 1$. This is perhaps because the transverse extents at the downstream pier showed greater variation with spacing, especially for pier combinations with intermediate relative diameter i.e., $D_d/D_u = 0.90$ and $D_d/D_u = 0.80$. For pier combinations with $D_d/D_u = 1.00$, the area variation mostly falls in line with longitudinal extent at the downstream pier. Thus, width seems to be the controlling factor for scour surface area variation at the downstream pier. Similar to variation of other scour hole dimensions at the downstream pier, the steepness of rise in the curve for scour surface area after $L/D_u > 8$ is highest for $D_d/D_u = 0.67$ followed by $D_d/D_u = 0.80$ followed by $D_d/D_u = 0.90$. Also, as observed for equilibrium scour depths and longitudinal extents, for unidentical piers, the point of minima seems to move upstream closer to the upstream pier with decrease in diameter of the downstream pier. Additionally, sharper minima points are observed for higher $D_d/D_u = 1.00$ and 0.90, while flatter (spread over a larger L/D_u range) minima are observed for pier combinations with lower sized downstream piers, i.e., $D_d/D_u = 0.80$ and 0.67. The trends of volume at the downstream pier are controlled mostly by the trends of area and depth at the downstream pier. Interestingly, single sharp minima points with a single value of L/D_u are observed for the normalized scour hole volumes at the downstream pier, and it is observed that the L/D_u of the minima decreases or minima occurs at a lower normalized spacing with the decrease in the diameter of the downstream pier, as shown in Table 4. This is because the smaller sized piers create a smaller sized hole and thus minima occur at a lower spacing between the piers. The upstream pier's hole gets larger length for its deposition to finish when the diameter of downstream pier is smaller.

Table 4. Spacings corresponding to the minimum scour hole volume at the downstream pier.

S. No.	D_d/D_u	L/D_u of minima of normalized scour hole volume at downstream piers
1	1.00	8.00
2	0.90	8.00
3	0.80	6.67
4	0.67	5.33

For convenience of application, polynomials are fit for the variation of normalized areal and volume extents of the upstream pier's hole, downstream pier's hole and the combined hole, and presented in supplementary Tables S1-S4, along with R^2 values.

3.1.5 Reinforcement Effect on the Upstream Pier

According to Fredsoe and Sumer (2002), the increase in the scour depth around the upstream pier can partly be due to the increase in horseshoe vortex flow. It was reported that for lower spacings, the presence of the downstream pier caused blockage of flow, resulting in an increase in the width of lee-wake vortices, shown in Fig. 1(a). Hence, a larger horseshoe vortex, formed in front of upstream pier, resulting in a larger scour depth. However, this is not the complete story. The physical interaction of the scour holes of the upstream and downstream piers plays a much greater role in the reinforcement effect, as it is not only the eroding forces that govern the magnitude of scour but also the ease with which the eroded sediments are able to exit the scour hole in the wake of the pier (Hannah, 1978)). The scour hole of the downstream pier pushes the peak of the mound between the piers downwards and upstream closer to the front pier. This changes the exit slope at the downstream side of front pier as shown in Fig. 1 (b). The downward movement of peak attempts to reduce the exit slope, making it easier for the eroded sediments from the upstream pier to cross the peak, thus enhancing the scour depth at the front pier. This downward movement or lowering of the bed level between the piers and the resulting decrease in exit slope is dominant and reported to be the root cause of reinforcement effect at the front pier by various studies (Hannah,1978; Nazariha, 1996). Therefore, all cases of relative diameter from $D_d/D_u = 0.67\ to\ 1.00$, report larger scour hole dimensions at the upstream pier compared to isolated piers.

A bigger sized downstream pier would result in a greater increase in the width of lee-wake vortices, resulting in a larger horseshoe vortex at the upstream pier and larger scour depth. Additionally, larger sized downstream piers lower the bed level between the piers to greater extents, resulting in greater reinforcement effect at the upstream pier. These two factors explain the order of reinforcement effect for unidentical piers, i.e., $D_d/D_u = 0.90 > D_d/D_u = 0.80 > D_d/D_u = 0.67$. However, the upstream pier in the case of $D_d/D_u = 1.00$ shows lower reinforcement effect than expected. This is because a larger sized downstream pier also moves the peak further upstream and thus dampens the decrease in exit slope, eventually reducing the magnitude of reinforcement effect to varying degrees. This upstream movement is naturally most significant for the largest sized downstream pier, i.e., $D_d/D_u = 1.00$, as seen through the lowest values of x_p for $D_d/D_u = 1.00$ in Fig. 6. Thus, the reinforcement effect is reduced for $D_d/D_u = 1.00$, compared to other cases.

4 APPLICATION IN BRIDGE PIER DESIGN

The piers of the newly constructed bridge if constructed downstream of an existing bridge should be given maximum sheltering. Thus, it is desirable to use downstream pier of as lower diameter as possible relative to the upstream pier, as shielding effect is highest for lowest D_d/D_u, at the same time ensuring that the piers are large enough to carry the anticipated loads on the new bridge. Based on the chosen D_d/D_u, Table 4 can be used as a guideline to decide the normalized spacing, i.e., L/D_u value at which the piers of the newly constructed bridge should be placed. The requirement of extra dimensions for foundation at the downstream pier is governed by the normalized scour hole dimensions at the downstream pier provided in Tables S1-S4. However, appropriate safety factors should be taken as the normalized scour depths at the downstream pier were observed to be sensitive to sediment coarseness. Additionally, for the decided spacing and relative pier diameter, degree of retrofitting measures at the upstream pier such as riprap extent, can be ascertained using scour hole dimensions at the upstream pier, provided in Tables S1 to S4, for the corresponding D_d/D_u and L/D_u.

If a new bridge with circular piers is to be constructed upstream of an existing bridge with piers larger or equal to existing bridge piers in size, it's piers should preferably be either of an identical size ($D_d/D_u = 1.00$) or a much larger size ($D_d/D_u = 0.67$), as they report the lowest reinforcement effects, and placed at sufficiently large normalized spacings where reinforcement effect is either minimal or absent, i.e., the normalized scour depth at the upstream pier approaches unity. Tables S1 to S4 can be used to decide the spacings. The downstream bridge piers will be always shielded by the upstream pier and thus no retrofitting measures would be required at the downstream pier due to the construction of upstream pier. Moreover, the downstream bridge piers would instead have additional protection due to the construction of the upstream bridge. Moreover, if the existing downstream pier was scour prone due to flow in the past, the newly placed upstream piers can be placed at suitable distance so as to shield the downstream pier well, a concept in line with sacrificial piles, at the same time ensuring that reinforcement effects at the upstream pier are minimized.

It is important to note that these recommendations are made based on experiments conducted at $U/U_c = 0.67$. For higher inflow velocities, other studies in literature can be referred. For instance, Table 2 can be used as a guide for locating the downstream pier in case of identical tandem piers as per the prevalent U/U_c.

5 CONCLUSIONS

For most spacings, separate scour holes are observed for the upstream and downstream piers with prominent deposition mounds between the piers. For the upstream pier, highest reinforcement effects are observed for pier combinations with $D_d/D_u = 0.90$ and 0.80, which is reflected in increased scour hole dimensions around the upstream pier, compared to isolated condition. This reinforcement effect reduced with spacing causing the scour hole dimensions to decline. At the downstream pier, the scour hole dimensions were always less than isolated condition due to the sheltering effect of the upstream pier. As the sheltering effect decreases and sediment deposition became insignificant, the scour hole dimensions again increased. The spacing corresponding to the minimum scour hole dimensions at the downstream pier is found to decrease with the decrease in diameter of the downstream pier. The location of the peak between the piers is found to shift downstream and upwards with the increase in the normalized spacing between the piers. It is seen that the contribution of the upstream pier to the combined area and volume of the scour hole is significantly higher than the downstream pier. Empirical polynomial Equations for normalized maximum scour depth, lateral and longitudinal extents, scour surface area and scour hole volume at varied spacings are presented in the form of supplementary tables S1 to S4 for four different ratios of upstream and downstream piers. It is desirable to use downstream pier of as lower diameter as possible relative to the upstream pier, as shielding effect is highest for lowest D_d/D_u. Table 4 can be used as a guideline to decide the normalized spacing, i.e., L/D_u value at which the downstream piers of the newly constructed bridge should be placed.

Notations:

h = flow depth (m).
L_e = longitudinal extent of the scour hole (mm).
T_u = transverse extent of the scour hole at the upstream pier (mm).
T_d = transverse extent of the scour hole at the downstream pier (mm).
A = areal extent of the scour hole (mm^2).
V = volume of the scour hole (mm^3).
U = mean flow velocity upstream of the pier (m/s).
U_c = critical velocity of sediment entrainment (m/s).
D_u = diameter of the upstream pier (mm).
D_d = diameter of the downstream pier (mm).
$A_{piers} = \pi \frac{{D_u}^2}{4} + \pi \frac{{D_d}^2}{4}$ = area of the piers (mm^2).
$V_{piers} = \pi \frac{{D_u}^2}{4} \times d_{seu} + \pi \frac{{D_d}^2}{4} \times d_{sed}$ = volume of the piers intercepting the flow at equilibrium (mm^3).
d_{sei} = equilibrium scour depth at the front of isolated pier (mm).
O = origin (0,0,0) at the centre of upstream/isolated pier and on the surface of the bed.
X = coordinate along flow direction in the plane of sand bed with origin O.
Y = coordinate perpendicular to the flow direction in the plane of sand bed with origin O.
Z = coordinate perpendicular to the plane of the sand bed with origin O.
d = scour depth at any point (X, Y, Z) (mm).
L = center to center spacing between two piers in tandem arrangement (mm).
d_{seu} = scour depth at the front of upstream pier for two piers in tandem arrangement (mm).
d_{sed} = scour depth at the front of downstream pier for two piers in tandem arrangement (mm)
D = diameter of identical piers in tandem arrangement (mm).
$D_{piers} = D_u + D_d$ = sum of diameters of upstream and downstream piers (mm).
D/d_{50} = sediment coarseness, i.e., the ratio of pier size to median sediment size.

REFERENCES

Arneson, L.A., Zevenbergen, L.W., Lagasse, P.F., Clopper, P.E., 2012. Evaluating scour at bridges (No. FHWA-HIF-12-003). National Highway Institute (US).
Ashtiani, B., Beheshti, A.A., 2006. Experimental investigation of clear-water local scour at pile groups. Journal of Hydraulic Engineering, 132(10), pp.1100-1104.
Beg, M., Beg, S., 2015. Scour hole characteristics of two unequal size bridge piers in tandem arrangement. ISH Journal of Hydraulic Engineering, 21(1), pp.85-96.
Beg, M., 2004. Mutual interference of bridge piers on local scour. In Proceedings of the Second International Conference on Scour and Erosion, Singapore (pp. 111-118).
Beg, M., 2008. Effect of mutual interference of bridge piers on local scour. In Department Of Civil Engineering. 2008. Aligarh Muslim University: Aligarh India. https://shodhganga.inflibnet.ac.in/handle/10603/246930
Chiew, Y.M., 1995. Mechanics of riprap failure at bridge piers. Journal of hydraulic engineering, 121(9), pp.635-643.
Devi, G., Kumar, M., 2022. Experimental study of the local scour around the two piers in the tandem arrangement using ultrasonic ranging transducers. Ocean Engineering, 266, p.112838
Dietz, J.W., 1973. Kolkbildung an einem kreiszylindrischen pfeilerpaar. Bautechnik, 50(6).
Dongguang, G., Pasada, L., Nordin, C.F., 1993. Pier scour equations used in the people's republic of china: review and summary.
Ettema, R., 1980. Scour at bridge piers.
Fredsoe, J., Sumer, B.M., 2002. The mechanics of scour in the marine environment (Vol. 17). World Scientific Publishing Company.
Hannah, C.R., 1978. Scour at pile groups. University of Canterbury, NZ. Civil Engineering, Research Report, 92.
Harshvardhan, Kaushal, D. R., 2025. Experimental study on the equilibrium scour pattern around isolated piers of varying diameter and inflow velocity. Particulate Science and

Technology, 1–15. https://doi.org/10.1080/02726351.2025.2494042
Kehsavarzi, A., Shrestha, C.K., Melville, B., Khabbaz, H., Ranjbar-Zahedani, M., Ball, J., 2018. Estimation of maximum scour depths at upstream of front and rear piers for two in-line circular columns. Environmental Fluid Mechanics, 18, pp.537-550.
Khaple, S., Hanmaiahgari, P.R., Gaudio, R., Dey, S., 2017. Interference of an upstream pier on local scour at downstream piers. Acta Geophysica, 65, pp.29-46.
Malik, R., Setia, B., 2021. Local scour around closely placed bridge piers. ISH Journal of Hydraulic Engineering, 27(4), pp.396-403.
Melville, B.W., Chiew, Y.M., 1999. Time scale for local scour at bridge piers. Journal of Hydraulic Engineering, 125(1), pp.59-65.
Melville, B.W., Coleman, S.E., 2000. Bridge scour. Water Resources Publication
Nazariha, M., 1996. Design relationships for maximum local scour depth for bridge pier groups. University of Ottawa (Canada).
Rahul, 2021. Interference Studies Around Bridge piers. National Institute of Technology, Kurukshetra.
Schlichting, H., Gersten, K., 1979. Boundary-layer theory 7th ed. In Kestin J. Chs. 14 and 20. New York: McGraw-hill.
Sheppard, D.M., Odeh, M., Glasser, T., 2004. Large scale clear-water local pier scour experiments. Journal of Hydraulic Engineering, 130(10), pp.957-963.
Yanmaz, A.M., Köse, Ö., 2007. Surface characteristics of scouring at bridge elements. Turkish Journal of Engineering & Environmental Sciences, 31(2).

Received 21 September 2025
Accepted 4 December 2025

Supplementary files

Table S1. Equations of scour hole dimensions for $D_d/D_u = 1$.

Parameter	Variation with L/D_u	L/D_u	R^2
d_{seu}/d_{sei}	$-0.0357 \times L/D_u + 1.1905$	$4 \le L/D_u \le 5\frac{1}{3}$	1
	1	$L/D_u \ge 5\frac{1}{3}$	
d_{sed}/d_{sei}	$0.0017 \times (L/D_u)^3 - 0.0201 \times (L/D_u)^2 + 0.0595 \times L/D_u + 0.5524$	$4 \le L/D_u \le 9\frac{1}{3}$	0.924
L_e/D_{piers}	$0.0246 \times (L/D_u)^3 - 0.4158 \times (L/D_u)^2 + 2.1321 \times L/D_u + 0.2048$	$4 \le L/D_u \le 9\frac{1}{3}$	0.969
L_u/D_{up}	$0.098 \times (L/D_u)^3 - 2.1375 \times (L/D_u)^2 + 15.08 \times L/D_u - 30.267$	$5\frac{1}{3} \le L/D_u \le 9\frac{1}{3}$	1
L_d/D_{dp}	$0.2062 \times (L/D_u)^2 - 2.795 \times L/D_u + 11.647$	$5\frac{1}{3} \le L/D_u \le 9\frac{1}{3}$	0.999
x_p/D_u	$-0.0422 \times (L/D_u)^3 + 0.8116 \times (L/D_u)^2 - 4.4214 \times L/D_u + 9.939$	$4 \le L/D_u \le 9\frac{1}{3}$	0.999
h_p/D_u	$-0.0321 \times (L/D_u)^2 + 0.6386 \times L/D_u - 2.1276$	$4 \le L/D_u \le 9\frac{1}{3}$	0.989
T_u/D_u	$-0.0258 \times (L/D_u)^3 + 0.5746 \times (L/D_u)^2 - 4.1774 \times L/D_u + 13.956$	$4 \le L/D_u \le 9\frac{1}{3}$	0.982
T_d/D_d	$-0.0914 \times (L/D_u)^3 + 1.7371 \times (L/D_u)^2 - 10.211 \times L/D_u + 21.676$	$4 \le L/D_u \le 9\frac{1}{3}$	0.934
A/A_{piers}	$0.0743 \times (L/D_u)^3 - 1.3635 \times (L/D_u)^2 + 8.0727 \times L/D_u + 1.1041$	$4 \le L/D_u \le 9\frac{1}{3}$	0.983
A_u/A_{up}	$0.641 \times (L/D_u)^3 - 13.93 \times (L/D_u)^2 + 98.19 \times L/D_u - 203.3$	$5\frac{1}{3} \le L/D_u \le 9\frac{1}{3}$	1
A_d/A_{dp}	$-0.378 \times (L/D_u)^3 + 8.65 \times (L/D_u)^2 - 63.46 \times L/D_u + 161.5$	$5\frac{1}{3} \le L/D_u \le 9\frac{1}{3}$	1
V/V_{piers}	$0.07 \times (L/D_u)^4 - 1.84 \times (L/D_u)^3 + 17.29 \times (L/D_u)^2 - 69.92 \times L/D_u + 109.31$	$4 \le L/D_u \le 9\frac{1}{3}$	1
V_u/V_{up}	$0.184 \times (L/D_u)^3 - 4.10 \times (L/D_u)^2 + 29.54 \times L/D_u - 61.74$	$5\frac{1}{3} \le L/D_u \le 9\frac{1}{3}$	1
V_d/V_{dp}	$0.314 \times (L/D_u)^3 - 6.69 \times (L/D_u)^2 + 46.48 \times L/D_u - 98.88$	$5\frac{1}{3} \le L/D_u \le 9\frac{1}{3}$	1

Table S2. Equations of scour hole dimensions for $D_d/D_u = 0.90$.

Parameter	Variation with L/D_u	L/D_u	R^2
d_{seu}/d_{sei}	$-0.0714 \times L/D_u + 1.4286$	$4 \le L/D_u \le 5\frac{1}{3}$	1
	1.0476	$5\frac{1}{3} \le L/D_u \le 9\frac{1}{3}$	
d_{sed}/d_{sei}	$0.0088 \times (L/D_u)^3 - 0.1718 \times (L/D_u)^2 + 1.0277 \times L/D_u - 1.3257$	$4 \le L/D_u \le 9\frac{1}{3}$	0.999
L_e/D_{piers}	$0.0333 \times (L/D_u)^3 - 0.6351 \times (L/D_u)^2 + 3.7312 \times L/D_u - 2.7669$	$4 \le L/D_u \le 9\frac{1}{3}$	0.964
L_u/D_{up}	$0.0375 \times (L/D_u)^3 - 0.7687 \times (L/D_u)^2 + 5.0083 \times L/D_u - 5.4$	$5\frac{1}{3} \le L/D_u \le 9\frac{1}{3}$	1
L_d/D_{dp}	$0.094 \times (L/D_u)^3 - 1.938 \times (L/D_u)^2 + 12.861 \times L/D_u - 24.815$	$5\frac{1}{3} \le L/D_u \le 9\frac{1}{3}$	1
x_p/D_u	$0.0589 \times (L/D_u)^2 - 0.1157 \times L/D_u + 2.2095$	$4 \le L/D_u \le 9\frac{1}{3}$	0.999
h_p/D_u	$-0.0241 \times (L/D_u)^2 + 0.5864 \times L/D_u - 2.299$	$4 \le L/D_u \le 9\frac{1}{3}$	0.999
T_u/D_u	$-0.0211 \times (L/D_u)^3 + 0.5237 \times (L/D_u)^2 - 4.1821 \times L/D_u + 15.749$	$4 \le L/D_u \le 9\frac{1}{3}$	0.974
T_d/D_d	$0.026 \times (L/D_u)^3 - 0.3839 \times (L/D_u)^2 + 1.7672 \times L/D_u + 1.109$	$4 \le L/D_u \le 9\frac{1}{3}$	0.847
A/A_{piers}	$0.0265 \times (L/D_u)^3 - 0.0041 \times (L/D_u)^2 - 3.953 \times L/D_u + 40.04$	$4 \le L/D_u \le 9\frac{1}{3}$	0.940
A_u/A_{up}	$-0.265 \times (L/D_u)^3 + 6.125 \times (L/D_u)^2 - 46.47 \times L/D_u + 145.13$	$5\frac{1}{3} \le L/D_u \le 9\frac{1}{3}$	1
A_d/A_{dp}	$1.008 \times (L/D_u)^3 - 21.44 \times (L/D_u)^2 + 149.37 \times L/D_u - 328.4$	$5\frac{1}{3} \le L/D_u \le 9\frac{1}{3}$	1
V/V_{piers}	$-0.0712 \times (L/D_u)^3 + 1.6932 \times (L/D_u)^2 - 12.978 \times L/D_u + 40.581$	$4 \le L/D_u \le 9\frac{1}{3}$	0.996
V_u/V_{up}	$-0.1 \times (L/D_u)^3 + 2.36 \times (L/D_u)^2 - 18.26 \times L/D_u + 56.26$	$5\frac{1}{3} \le L/D_u \le 9\frac{1}{3}$	1
V_d/V_{dp}	$0.268 \times (L/D_u)^3 - 5.66 \times (L/D_u)^2 + 39.34 \times L/D_u - 85.74$	$5\frac{1}{3} \le L/D_u \le 9\frac{1}{3}$	1

Table S3. Equations of scour hole dimensions for $D_d/D_u = 0.80$.

Parameter	Variation with L/D_u	L/D_u	R^2
d_{seu}/d_{sei}	$-0.0714 \times L/D_u + 1.4286$	$4 \leq L/D_u \leq 5\frac{1}{3}$	1
	1.0476	$5\frac{1}{3} \leq L/D_u \leq 8$	
	$-0.0357 \times L/D_u + 1.3333$	$8 \leq L/D_u \leq 9\frac{1}{3}$	
d_{sed}/d_{sei}	$0.0062 \times (L/D_u)^3 - 0.1052 \times (L/D_u)^2 + 0.52 \times L/D_u - 0.1445$	$4 \leq L/D_u \leq 9\frac{1}{3}$	0.982
L_e/D_{piers}	$0.0182 \times (L/D_u)^3 - 0.3125 \times (L/D_u)^2 + 1.5787 \times L/D_u + 1.5926$	$4 \leq L/D_u \leq 9\frac{1}{3}$	1
L_u/D_{up}	$-0.0563 \times (L/D_u)^3 + 1.275 \times (L/D_u)^2 - 9.6 \times L/D_u + 28.533$	$5\frac{1}{3} \leq L/D_u \leq 9\frac{1}{3}$	1
L_d/D_{dp}	$0.111 \times (L/D_u)^3 - 2.2969 \times (L/D_u)^2 + 15.552 \times L/D_u - 32.08$	$5\frac{1}{3} \leq L/D_u \leq 9\frac{1}{3}$	1
x_p/D_u	$-0.0536 \times (L/D_u)^2 + 1.2943 \times L/D_u - 1.6305$	$4 \leq L/D_u \leq 9\frac{1}{3}$	0.985
h_p/D_u	$-0.0141 \times (L/D_u)^3 + 0.2491 \times (L/D_u)^2 - 1.1214 \times L/D_u + 1.2591$	$4 \leq L/D_u \leq 9\frac{1}{3}$	0.996
T_u/D_u	$0.0164 \times (L/D_u)^3 - 0.3549 \times (L/D_u)^2 + 2.2155 \times L/D_u + 0.9981$	$4 \leq L/D_u \leq 9\frac{1}{3}$	0.935
T_d/D_d	$0.1172 \times (L/D_u)^3 - 2.1261 \times (L/D_u)^2 + 12.109 \times L/D_u - 18.743$	$4 \leq L/D_u \leq 9\frac{1}{3}$	0.999
A/A_{piers}	$0.3317 \times (L/D_u)^3 - 6.3324 \times (L/D_u)^2 + 37.314 \times L/D_u - 46.113$	$4 \leq L/D_u \leq 9\frac{1}{3}$	0.970
A_u/A_{up}	$-0.0812 \times (L/D_u)^2 - 1.5642 \times L/D_u + 41.97$	$5\frac{1}{3} \leq L/D_u \leq 9\frac{1}{3}$	0.987
A_d/A_{dp}	$0.627 \times (L/D_u)^3 - 10.99 \times (L/D_u)^2 + 59.90 \times L/D_u - 90.76$	$5\frac{1}{3} \leq L/D_u \leq 9\frac{1}{3}$	1
V/V_{piers}	$0.0415 \times (L/D_u)^3 - 0.8696 \times (L/D_u)^2 + 5.3225 \times L/D_u - 1.0742$	$4 \leq L/D_u \leq 9\frac{1}{3}$	0.894
V_u/V_{up}	$-0.169 \times (L/D_u)^3 + 3.82 \times (L/D_u)^2 - 29.02 \times L/D_u + 82.54$	$5\frac{1}{3} \leq L/D_u \leq 9\frac{1}{3}$	1
V_d/V_{dp}	$-0.255 \times (L/D_u)^3 + 5.94 \times (L/D_u)^2 - 44.54 \times L/D_u + 111.42$	$5\frac{1}{3} \leq L/D_u \leq 9\frac{1}{3}$	1

Table S4. Equations of scour hole dimensions for $D_d/D_u = 0.67$.

Parameter	Variation with L/D_u	L/D_u	R^2
d_{seu}/d_{sei}	1.0476	$4 \leq L/D_u \leq 8$	1
	$-0.0357 \times L/D_u + 1.3333$	$8 \leq L/D_u \leq 9\frac{1}{3}$	
d_{sed}/d_{sei}	0.2857	$4 \leq L/D_u \leq 8$	1
	$0.2143 \times L/D_u - 1.4286$	$8 \leq L/D_u \leq 9\frac{1}{3}$	
L_e/D_{piers}	$0.0169 \times (L/D_u)^3 - 0.27 \times (L/D_u)^2 + 1.35 \times L/D_u + 1.128$	$4 \leq L/D_u \leq 9\frac{1}{3}$	0.989
L_u/D_{up}	$-0.033 \times (L/D_u)^4 + 0.88 \times (L/D_u)^3 - 8.45 \times (L/D_u)^2 + 34.83 \times L/D_u - 47.67$	$5\frac{1}{3} \leq L/D_u \leq 9\frac{1}{3}$	1
L_d/D_{dp}	$0.0562 \times (L/D_u)^3 - 0.9603 \times (L/D_u)^2 + 5.2411 \times L/D_u - 7.4343$	$5\frac{1}{3} \leq L/D_u \leq 9\frac{1}{3}$	0.972
x_p/D_u	$0.62 \times L/D_u + 0.4267$	$4 \leq L/D_u \leq 9\frac{1}{3}$	0.989
h_p/D_u	$-0.0295 \times (L/D_u)^2 + 0.5679 \times L/D_u - 1.5981$	$4 \leq L/D_u \leq 9\frac{1}{3}$	0.999
T_u/D_u	$-0.0281 \times (L/D_u)^3 + 0.5786 \times (L/D_u)^2 - 3.7143 \times L/D_u + 11.55$	$4 \leq L/D_u \leq 9\frac{1}{3}$	0.902
T_d/D_d	$0.1055 \times (L/D_u)^3 - 1.9125 \times (L/D_u)^2 + 11.212 \times L/D_u - 19.64$	$4 \leq L/D_u \leq 9\frac{1}{3}$	0.980
A/A_{piers}	$0.1347 \times (L/D_u)^3 - 2.1286 \times (L/D_u)^2 + 10.793 \times L/D_u - 2.8934$	$4 \leq L/D_u \leq 9\frac{1}{3}$	0.999
A_u/A_{up}	$-0.14 \times (L/D_u)^4 + 3.62 \times (L/D_u)^3 - 33.64 \times (L/D_u)^2 + 133.96 \times L/D_u + 173.2$	$5\frac{1}{3} \leq L/D_u \leq 9\frac{1}{3}$	1
A_d/A_{dp}	$0.751 \times (L/D_u)^3 - 13.36 \times (L/D_u)^2 + 76.47 \times L/D_u - 137.6$	$5\frac{1}{3} \leq L/D_u \leq 9\frac{1}{3}$	0.980
V/V_{piers}	$-0.0623 \times (L/D_u)^3 + 1.2743 \times (L/D_u)^2 - 8.1584 \times L/D_u + 22.653$	$4 \leq L/D_u \leq 9\frac{1}{3}$	0.889
V_u/V_{up}	$-0.036 \times (L/D_u)^4 + 0.90 \times (L/D_u)^3 - 8.18 \times (L/D_u)^2 + 31.74 \times L/D_u - 37.97$	$5\frac{1}{3} \leq L/D_u \leq 9\frac{1}{3}$	1
V_d/V_{dp}	$-0.0962 \times (L/D_u)^3 + 2.0722 \times (L/D_u)^2 - 13.591 \times L/D_u + 30.989$	$5\frac{1}{3} \leq L/D_u \leq 9\frac{1}{3}$	0.977

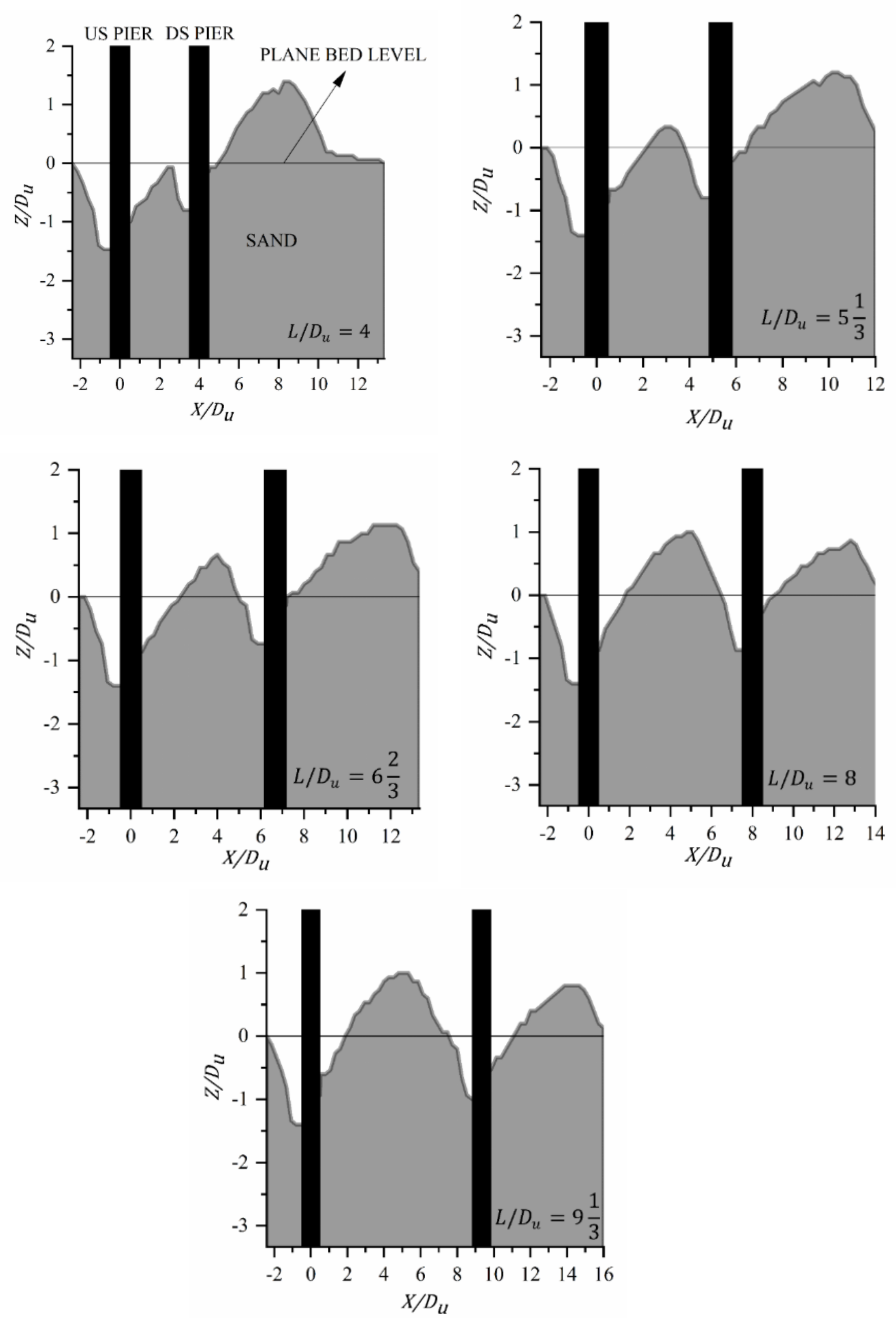

Fig. S1. Centreline scour profiles for $\frac{D_d}{D_u} = 1.0$ at $\frac{U}{U_c} = 0.67$ for L/D_u ranging from 4 to $9\frac{1}{3}$.

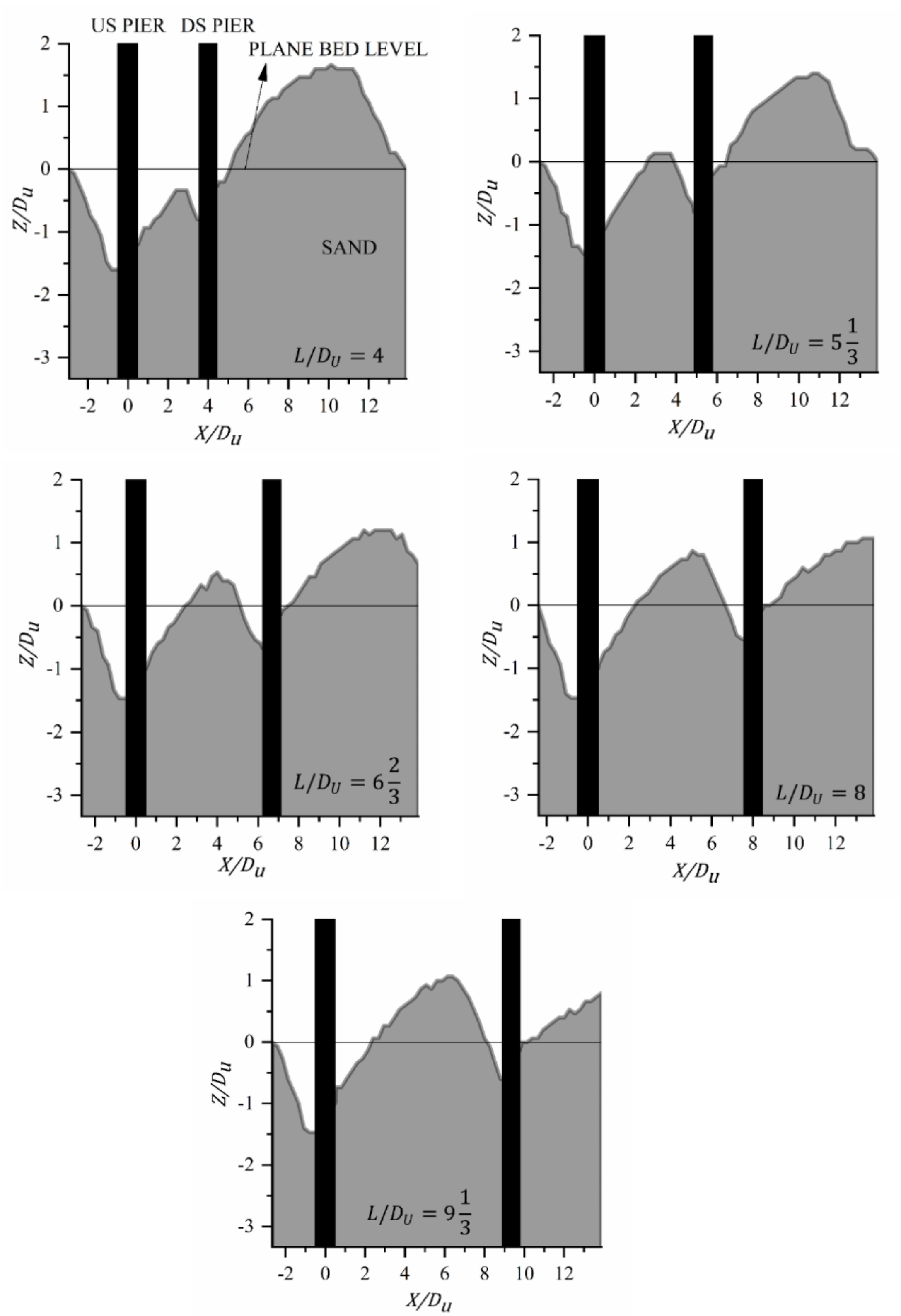

Fig. S2. Centreline scour profiles for $\frac{D_d}{D_u} = 0.9$ at $\frac{U}{U_c} = 0.67$ for L/D_u ranging from 4 to $9\frac{1}{3}$.

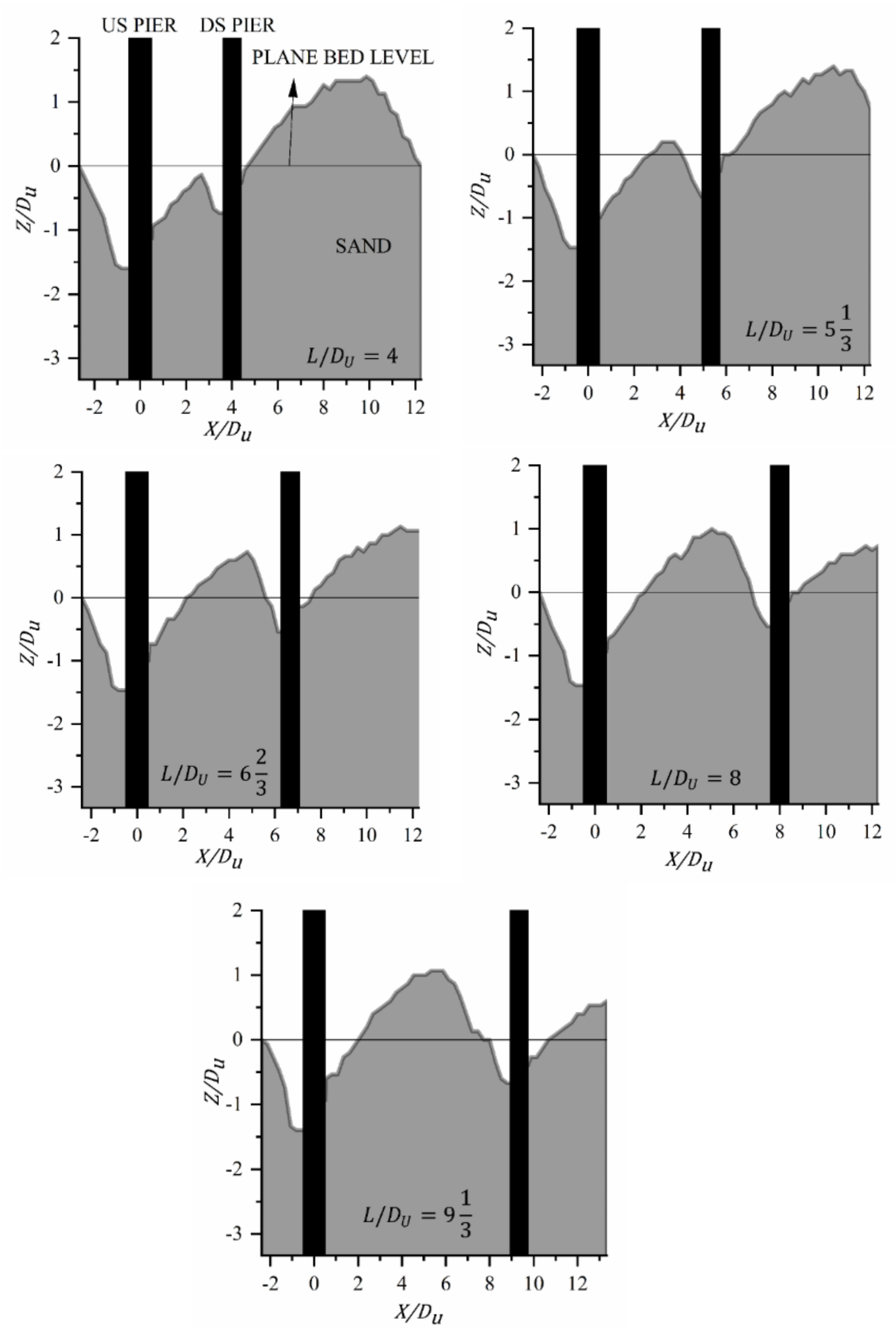

Fig. S3. Centreline scour profiles for $\frac{D_d}{D_u} = 0.8$ at $\frac{U}{U_c} = 0.67$ for L/D_u ranging from 4 to $9\frac{1}{3}$.

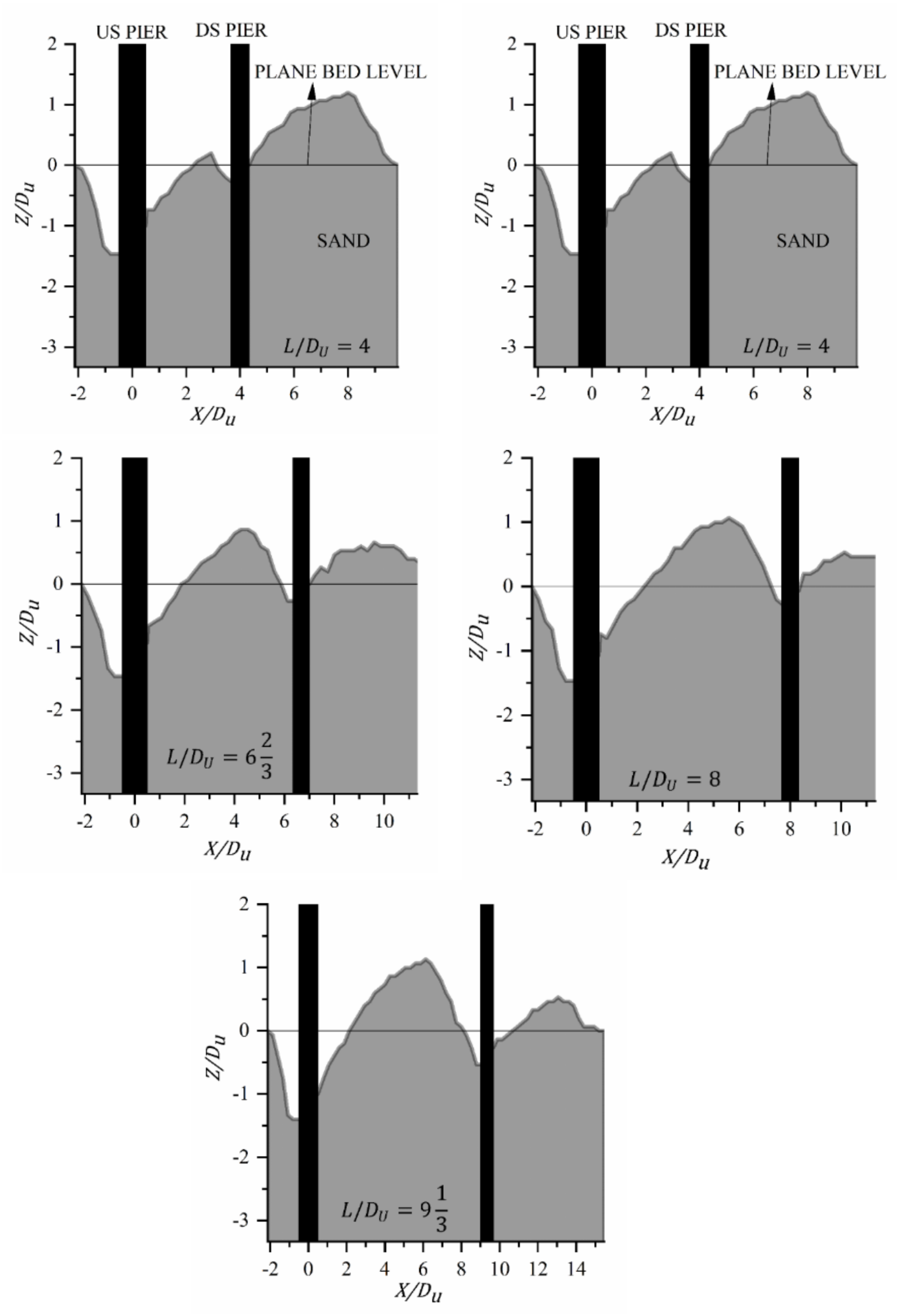

Fig. S4. Centreline scour profiles for $\frac{D_d}{D_u} = 0.67$ at $\frac{U}{U_c} = 0.67$ for L/D_u ranging from 4 to $9\frac{1}{3}$.

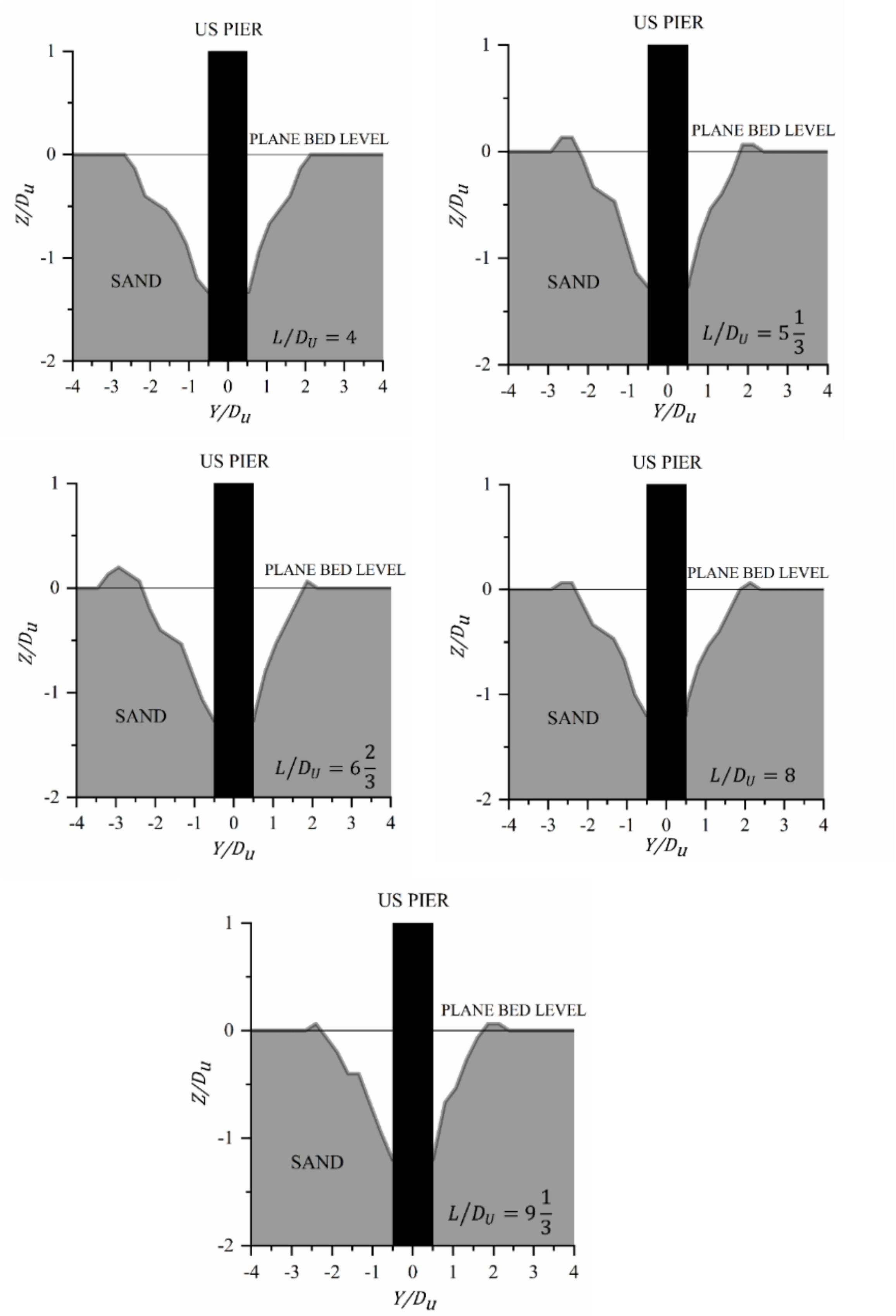

Fig. S5. Transverse scour profiles at the upstream pier for $\frac{D_d}{D_u} = 1$at $\frac{U}{U_c} = 0.67$ for L/D_u ranging from 4 to $9\frac{1}{3}$.

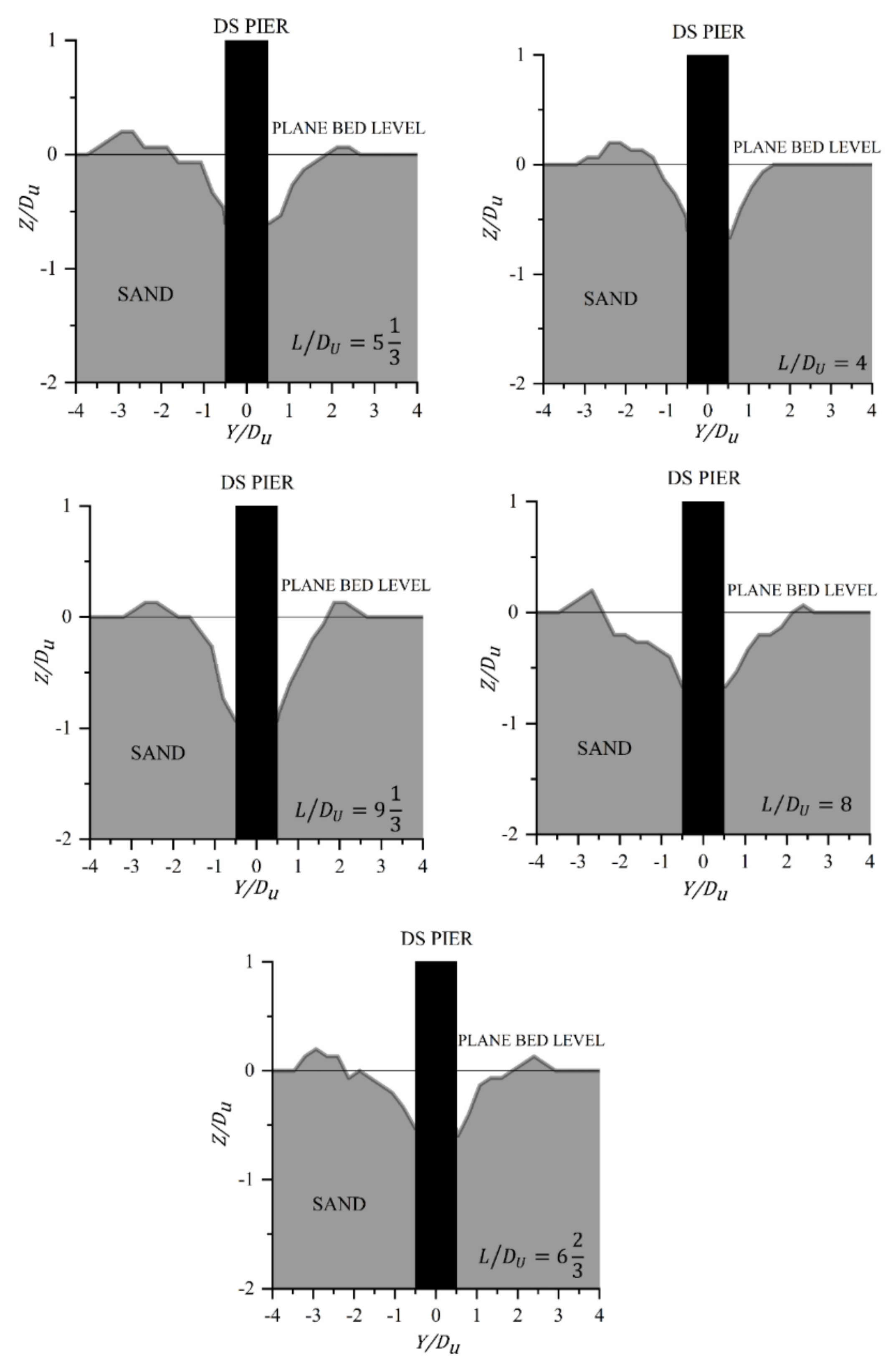

Fig. S6. Transverse scour profiles at the downstream pier for $\frac{D_d}{D_u} = 1$at $\frac{U}{U_c} = 0.67$ for L/D_u ranging from 4 to $9\frac{1}{3}$.

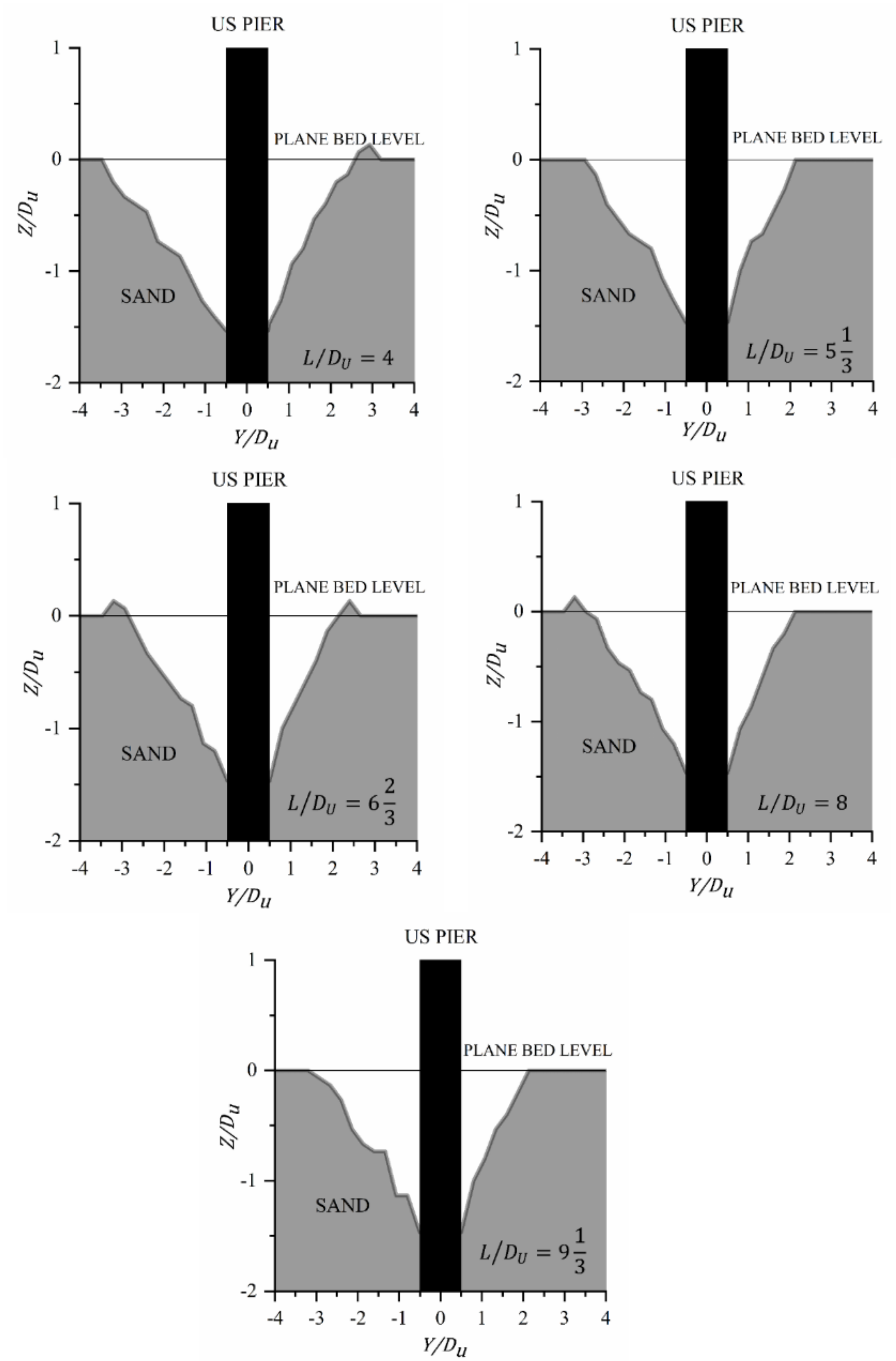

Fig. S7. Transverse scour profiles at the upstream pier for $\frac{D_d}{D_u} = 0.9$ at $\frac{U}{U_c} = 0.67$ for L/D_u ranging from 4 to $9\frac{1}{3}$.

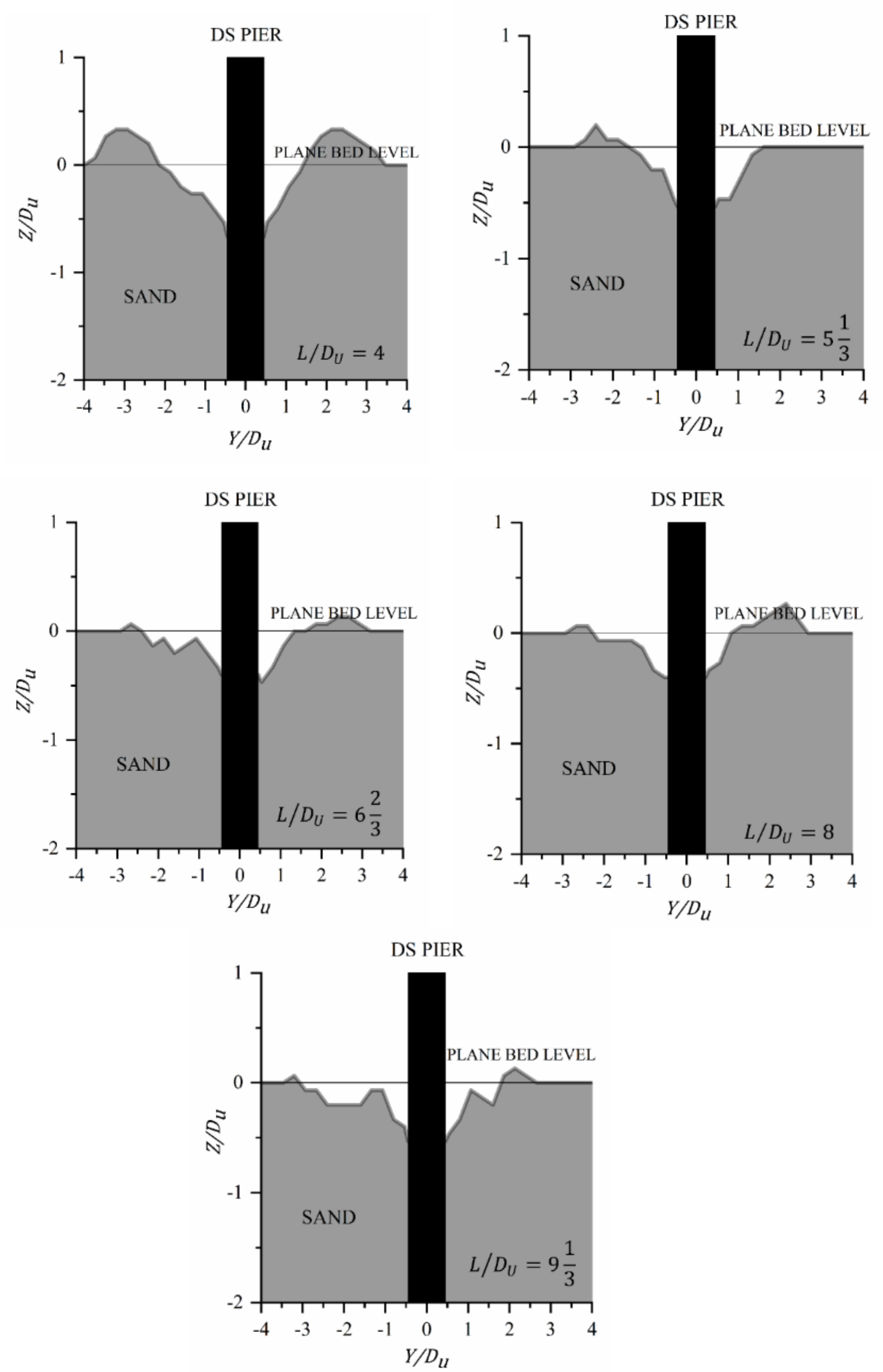

Fig. S8. Transverse scour profiles at the downstream pier for $\frac{D_d}{D_u} = 0.9$ at $\frac{U}{U_c} = 0.67$ for L/D_u ranging from 4 to $9\frac{1}{3}$.

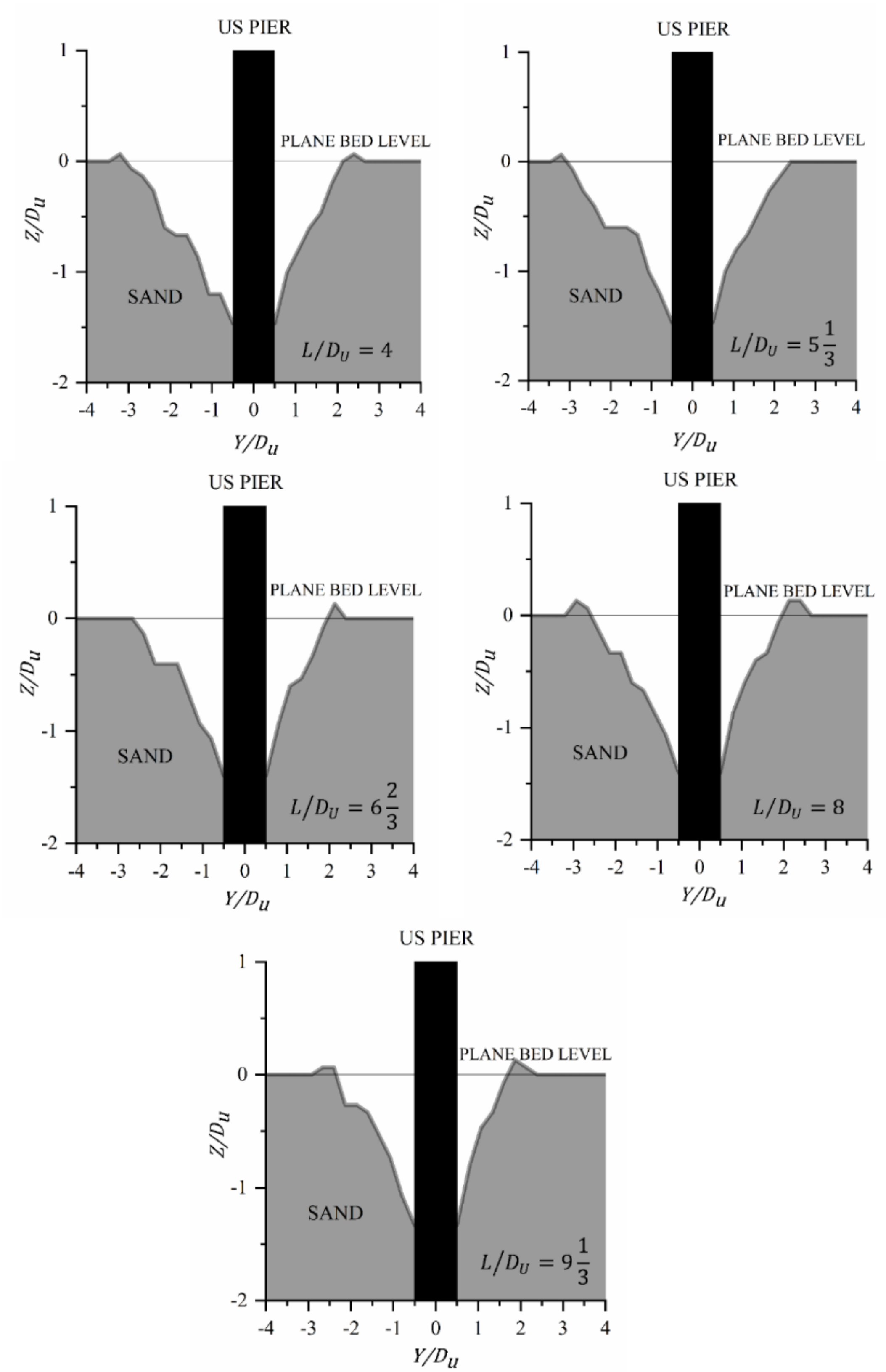

Fig. S9. Transverse scour profiles at the upstream pier for $\frac{D_d}{D_u} = 0.8$ at $\frac{U}{U_c} = 0.67$ for L/D_u ranging from 4 to $9\frac{1}{3}$.

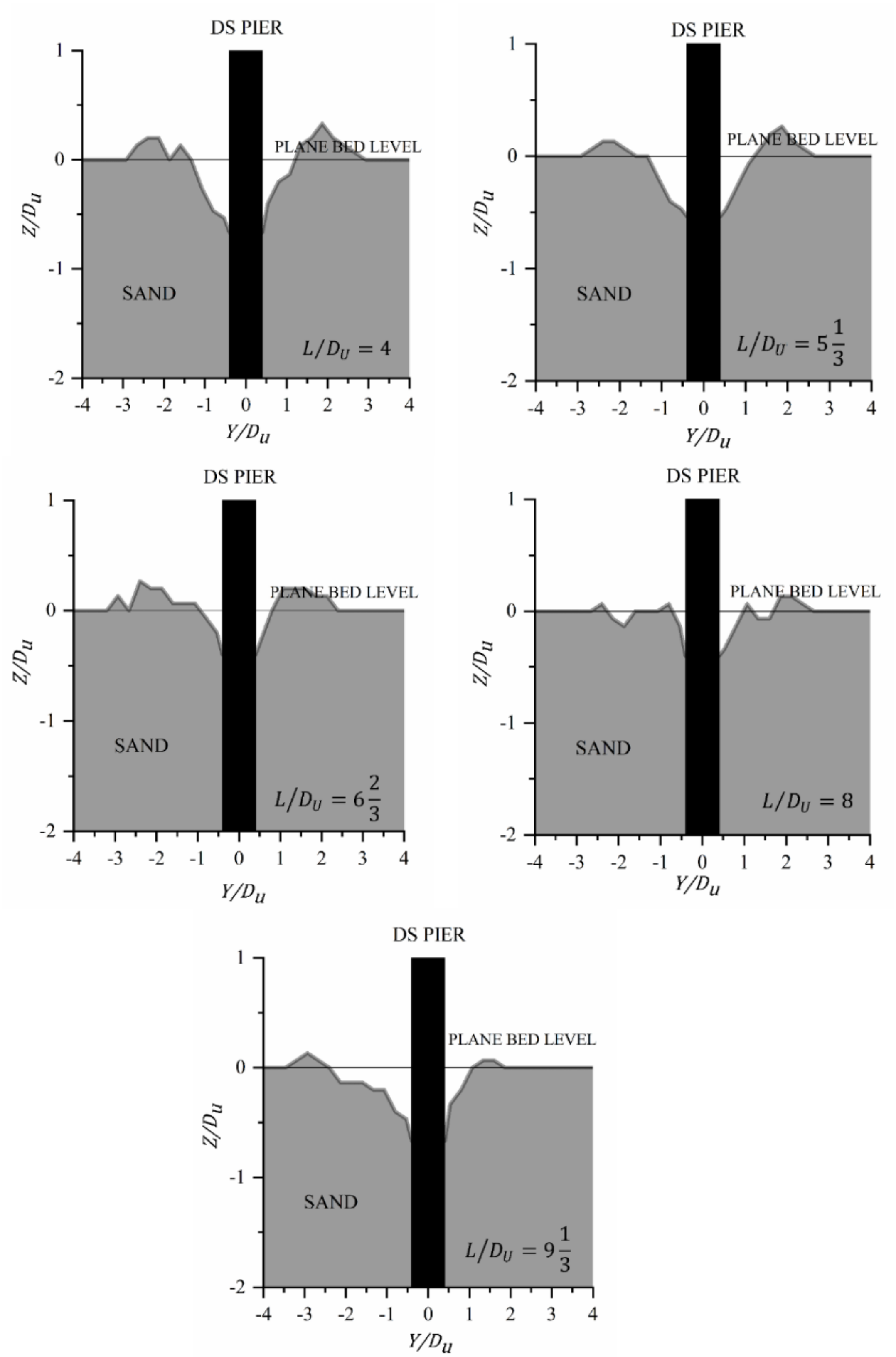

Fig. S10. Transverse scour profiles at the upstream pier for $\frac{D_d}{D_u} = 0.8$ at $\frac{U}{U_c} = 0.67$ for L/D_u ranging from 4 to $9\frac{1}{3}$.

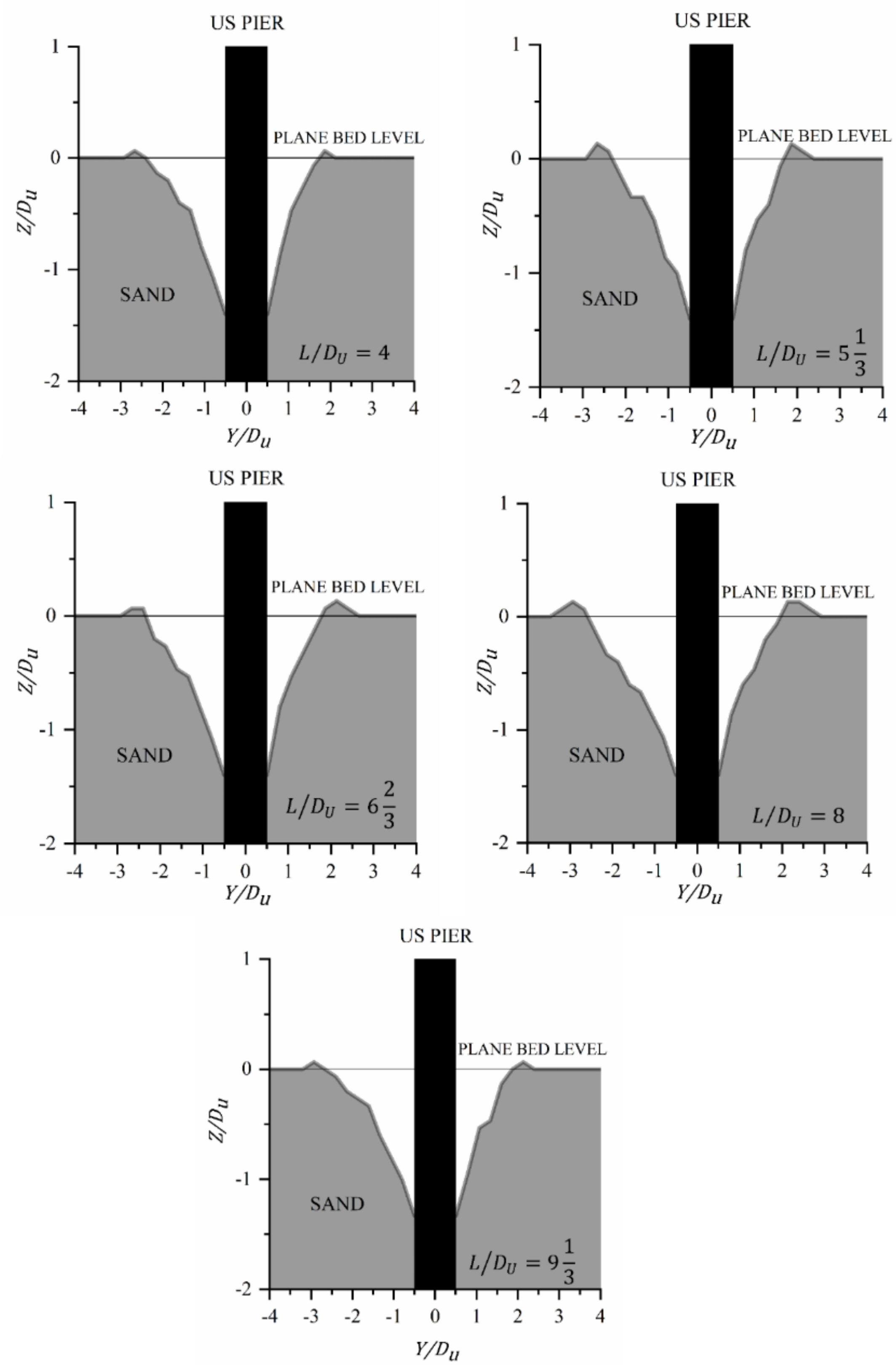

Fig. S11. Transverse scour profiles at the upstream pier for $\frac{D_d}{D_u} = 0.67$ at $\frac{U}{U_c} = 0.67$ for L/D_u ranging from 4 to $9\frac{1}{3}$.

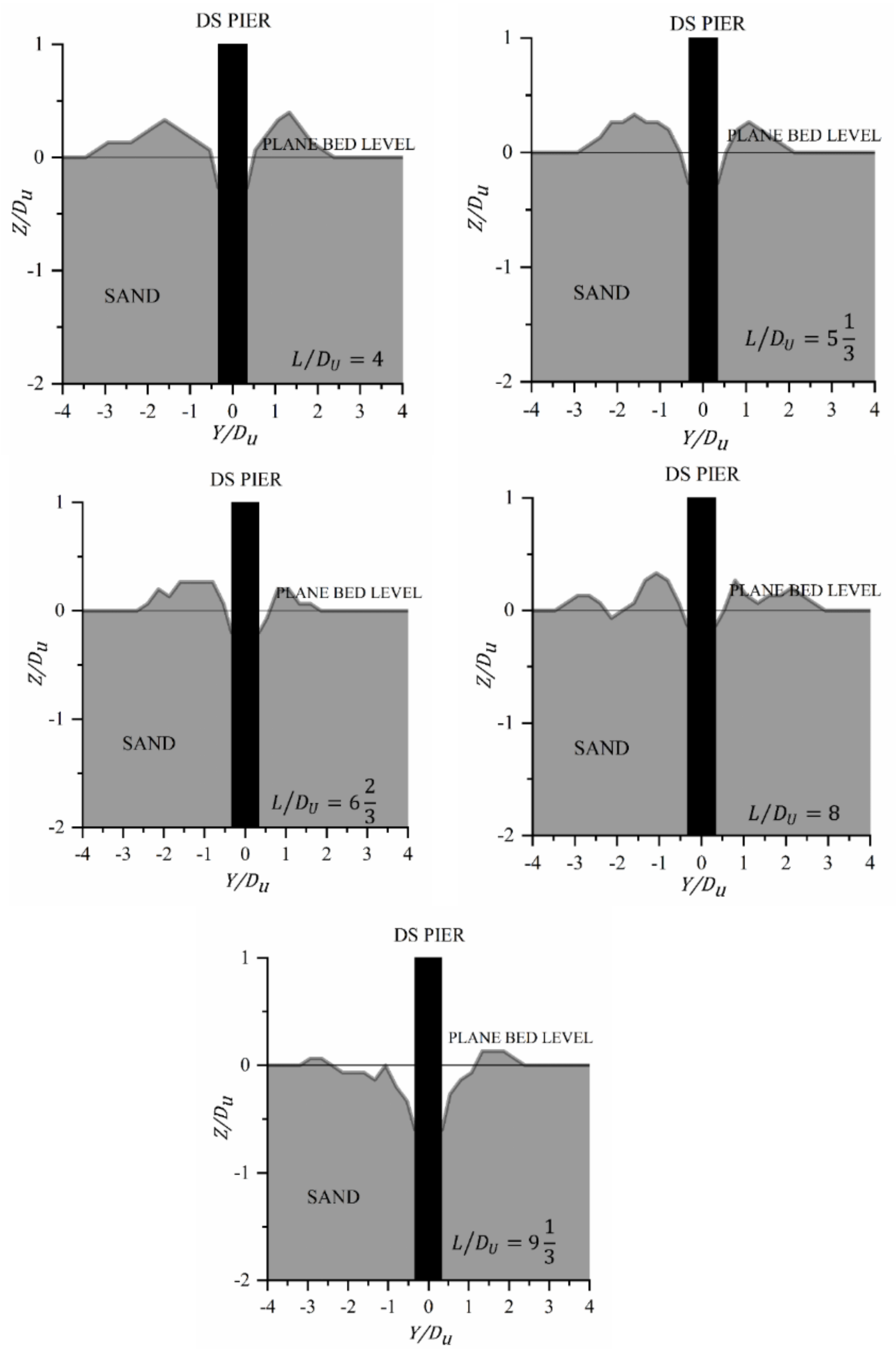

Fig. S12. Transverse scour profiles at the downstream pier for D_d/D_u =0.67 at U/U_c =0.67 for L⁄D_u ranging from 4 to 9 1/3.

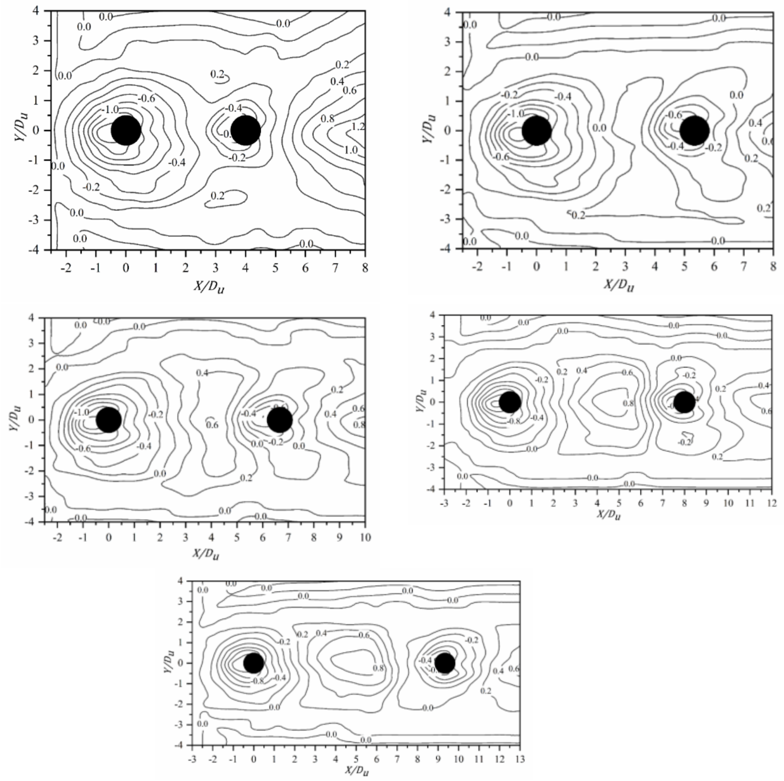

Fig. S13. Normalized Scour hole contours (d/D_u) around inline piers with $\frac{D_d}{D_u} = 1$ at $\frac{U}{U_c} = 0.67$ for L/D_u ranging from 4 to $9\frac{1}{3}$

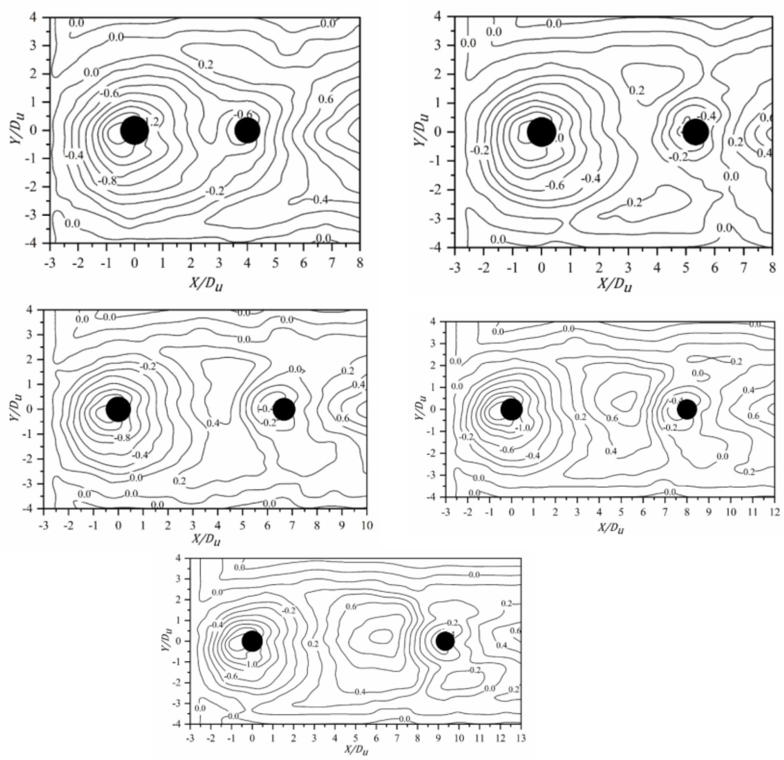

Fig. S14. Normalized Scour hole contours (d/D_u) around inline piers with $\frac{D_d}{D_u} = 0.9$ at $\frac{U}{U_c} = 0.67$ for L/D_u ranging from 4 to $9\frac{1}{3}$.

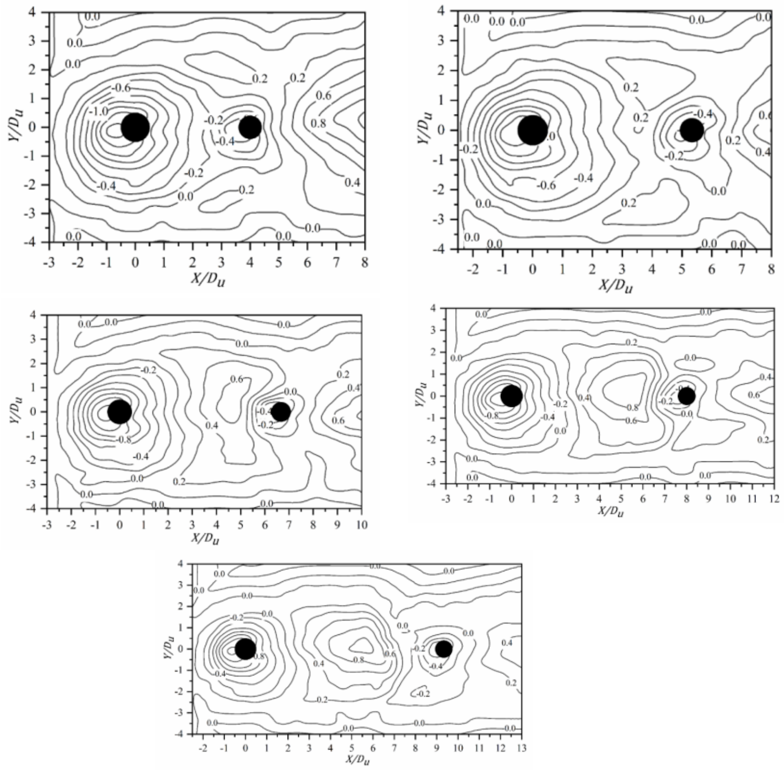

Fig. S15. Normalized Scour hole contours (d/D_u) around inline piers with $\frac{D_d}{D_u} = 0.8$ at $\frac{U}{U_c} = 0.67$ for L/D_u ranging from 4 to $9\frac{1}{3}$.

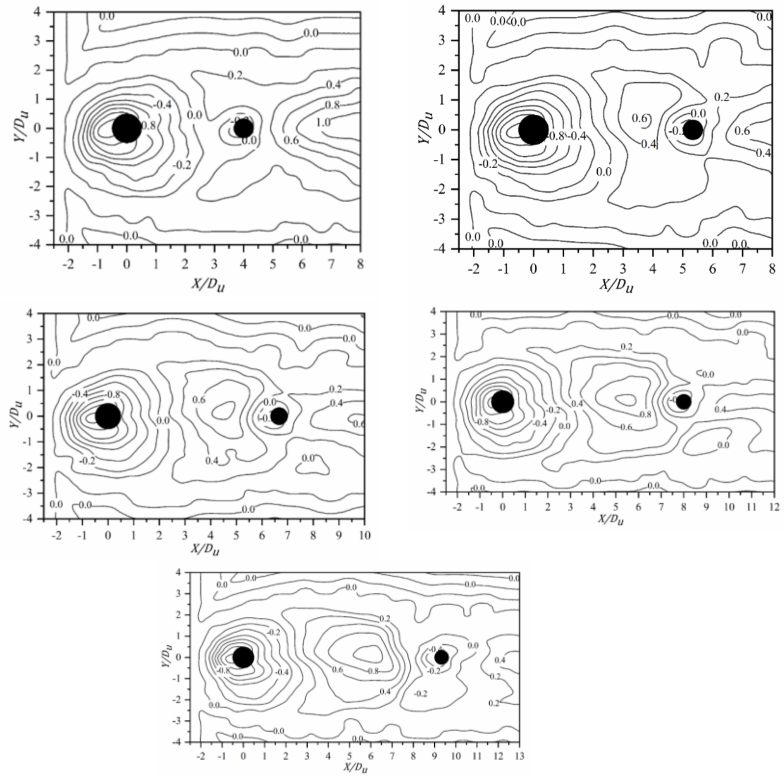

Fig. S16. Normalized Scour hole contours (d/D_u) around inline piers with $\frac{D_d}{D_u} = 0.67$ at $\frac{U}{U_c} = 0.67$ for L/D_u ranging from 4 to $9\frac{1}{3}$.

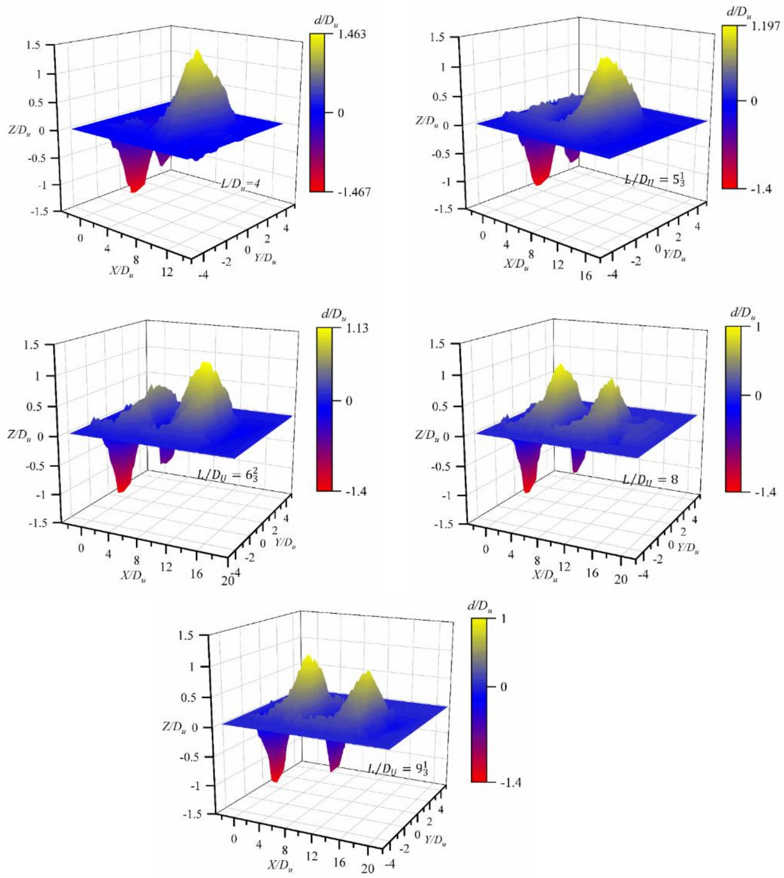

Fig. S17. Normalized 3-D Scour hole colour diagrams (d/D_u) around inline piers with $\frac{D_d}{D_u} = 1$ at $\frac{U}{U_c} = 0.67$ for L/D_u ranging from 4 to $9\frac{1}{3}$.

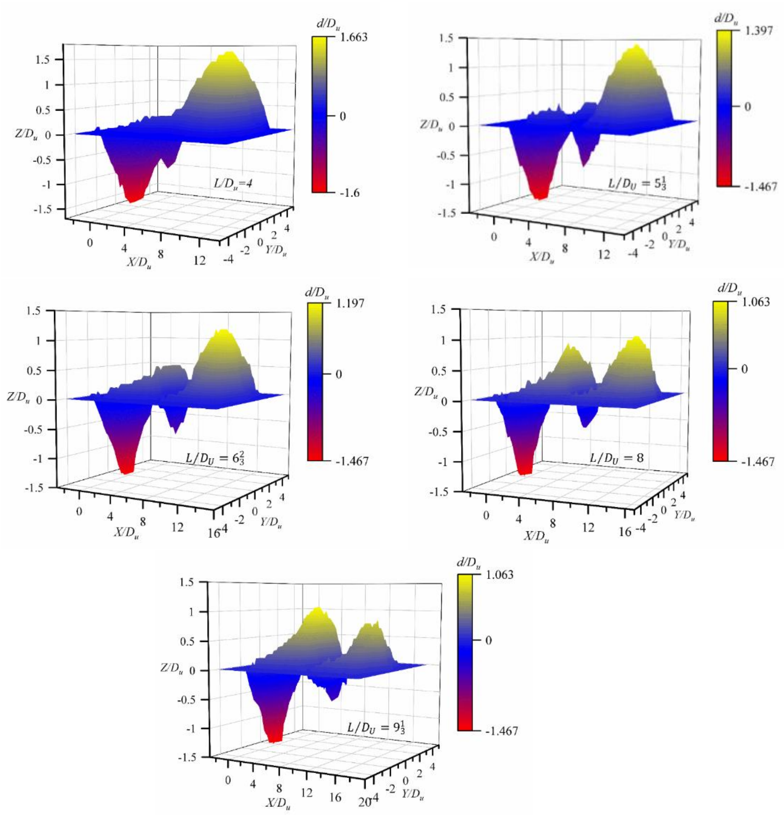

Fig. S18. Normalized 3-D Scour hole colour diagrams (d/D_u) around inline piers with $\frac{D_d}{D_u} = 0.9$ at $\frac{U}{U_c} = 0.67$ for L/D_u ranging from 4 to $9\frac{1}{3}$.

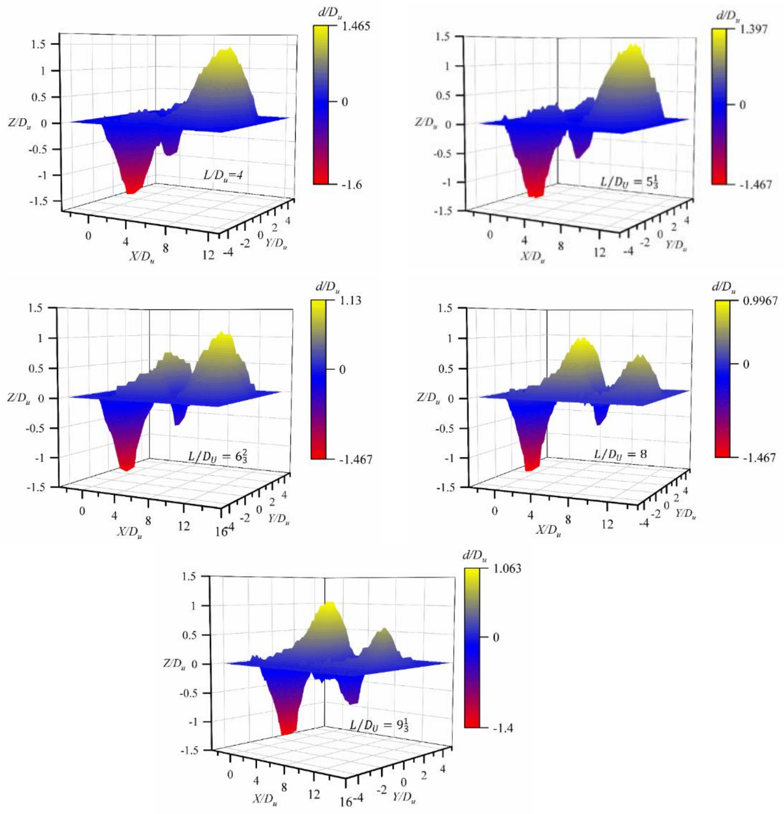

Fig. S19. Normalized 3-D Scour hole colour diagrams (d/D_u) around inline piers with $\frac{D_d}{D_u} = 0.8$ at $\frac{U}{U_c} = 0.67$ for L/D_u ranging from 4 to $9\frac{1}{3}$.

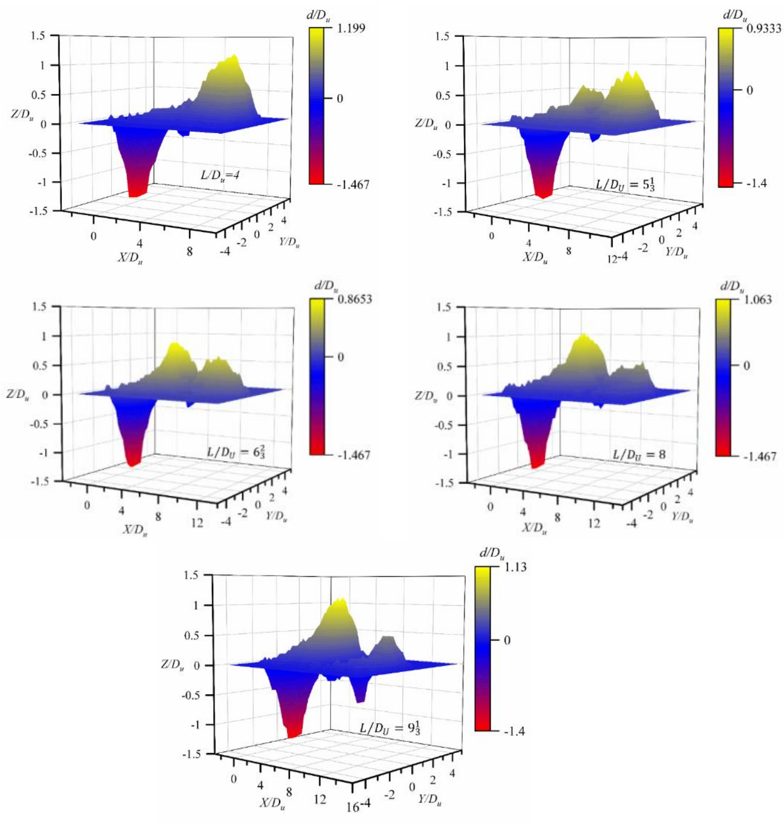

Fig. S20. Normalized 3-D Scour hole colour diagrams (d/D_u) around inline piers with $\frac{D_d}{D_u} = 0.67$ at $\frac{U}{U_c} = 0.67$ for L/D_u ranging from 4 to $9\frac{1}{3}$.